JOURNAL OF COMPUTATIONAL PHYSICS **123,** 15–31 (1996)
ARTICLE NO. 0002

Spectral Analysis of Resistive MHD in Toroidal Geometry

A. R. SCHELLHASE AND R. G. STORER

Department of Physics, The Flinders University of South Australia, G.P.O. Box 2100, Adelaide 5001, Australia

Received August 26, 1994; revised April 10, 1995

A code, SPECTOR, has been developed to determine the complete spectrum (both stable and unstable modes) for a resistive plasma in toroidal geometry described by the linearized, compressible, magnetohydrodynamic, single fluid equations. The structure of the code is explained and comparisons with other codes are presented which test its validity. Some applications to both cylindrical and tokamak-like plasmas are presented to illustrate the scope of the code particularly for the stable part of the spectrum. A study is made of the effect of resistivity on a typical toroidal Alfvén eigenmode.

1. INTRODUCTION

Numerical approaches to the study of stability using toroidal resistive magnetohydrodynamics (MHD) have been carried out for some time (Charlton *et al*. [1], Storer [2], Hughes *et al*. [3], Vlad *et al*. [4], and Kerner *et al*. [5]). These codes followed the significant development of the ideal MHD toroidal stability codes ERATO [6] and PEST [7]. The emphasis in most of these codes was on the study of the discrete unstable modes, particularly in the regions where ideal MHD would predict stability. Due to the analytic and numerical complexities of the analysis involved in these toroidal codes, simplifying assumptions were made in some early versions (e.g., incompressibility [1–3], reduced equations [8]). Non-linear time development has, to a large extent, been restricted to using the reduced equation set [8]. There has been a renewed interest in the study of the complete spectrum of resistive MHD, both because of the interesting structure of the stable, resistive spectrum (Ryu and Grimm [9], Kerner *et al*. [10–12], Dewar and Davies [13]) and through the recognition of the importance of toroidal Alfvén eigenmodes (Cheng and Chance [14], Poedts and Schwartz [15], Turnbull *et al*. [16], Kerner *et al*. [17]). We present in this paper a description of a code, SPECTOR (Schellhase [18]), which has been developed to study the spectrum of the linearized, compressible equations of resistive MHD in toroidal geometry. This code has been partially validated by comparison with a toroidal ideal code [6] and by a study of the stable spectra of cylindrical plasmas [9–13].

2. THE RESISTIVE MHD EQUATIONS

MHD is a single fluid description of a plasma. The MHD model is one of the simplest models for describing the interaction processes between a plasma and a magnetic field. At any point in space and time the macroscopic variables $\mathbf{v}$, $\mathbf{B}$, p, ρ (and η for the resistive case) describe the state of the system. $\mathbf{B}$ is the magnetic field, $\mathbf{v}$ is the macroscopic fluid velocity, p is the thermal pressure, η is the resistivity of the plasma, and ρ is the mass density. Γ is the ratio of specific heats. The following resistive MHD equations describe how this state changes in time:

$$\rho \frac{d\mathbf{v}}{dt} = \frac{1}{\mu_0}(\nabla \times \mathbf{B}) \times \mathbf{B} - \nabla p, \tag{1}$$

$$\frac{\partial \mathbf{B}}{\partial t} = \nabla \times (\mathbf{v} \times \mathbf{B}) - \frac{1}{\mu_0} \nabla \times (\eta \nabla \times \mathbf{B}), \tag{2}$$

$$\frac{\partial p}{\partial t} = -\mathbf{v} \cdot \nabla p - \Gamma p \nabla \cdot \mathbf{v}, \tag{3}$$

$$\frac{\partial p}{\partial t} = -\mathbf{v} \cdot \nabla \rho - \rho \nabla \cdot v, \tag{4}$$

$$\nabla \cdot \mathbf{B} = 0. \tag{5}$$

As they stand the resistive MHD equations are non-linear and consequently are extremely difficult to analyse theoretically. If we make the assumption that plasma stability can be investigated by considering infinitesimal perturbations around the equilibrium, we can focus our analysis on the linearised resistive MHD equations. Any perturbation may then be expressed as the sum of eigenfunctions, and these eigenfunctions are unique for any given equilibrium and boundary conditions. We recognise that non-linear effects are important in many situations; however, it is certainly also important to avoid linear instabilities and linear effects are important in identifying the stable modes which are excited by external influences. If we neglect the effects of the other transport coefficients and perturb the macroscopic variables according to, $\mathbf{Z} \Rightarrow \mathbf{Z} + \mathbf{z}$, where $\mathbf{Z}$ is the equilibrium value and $\mathbf{z}$ is the first-order perturbation value, and consider the zeroth- and first-order equations (assuming that the plasma has zero velocity at equilibrium), we obtain the standard MHD equilibrium equations,

0021-9991/96 $12.00

$$\mathbf{J} \times \mathbf{B} = \nabla P, \tag{6}$$

$$\nabla \times \mathbf{B} = \mu_0 \mathbf{J}, \tag{7}$$

$$\nabla \cdot \mathbf{B} = 0, \tag{8}$$

which are employed to determine the equilibrium state, and the linearised resistive MHD equations,

$$\frac{\partial \mathbf{v}}{\partial t} = (\nabla \times \mathbf{B}) \times \mathbf{b} + (\nabla \times \mathbf{b}) \times \mathbf{B} - \nabla p, \tag{9}$$

$$\frac{\partial \mathbf{b}}{\partial t} = \nabla \times (\mathbf{v} \times \mathbf{B}) - \nabla \times \eta (\nabla \times \mathbf{b}), \tag{10}$$

$$\frac{\partial p}{\partial t} = -\mathbf{v} \cdot \nabla P - \Gamma P \nabla \cdot \mathbf{v}. \tag{11}$$

which can be analysed with the equilibrium quantities to determine stability. In order to cast Eqs. (6)–(11) in this dimensionless form we introduce a characteristic field amplitude, B_0, which is chosen to be the toroidal magnetic field in the vicinity of the magnetic axis, and a characteristic length, the plasma radius r_p. With these choices we define the time scale to be the toroidal Alfvén transit time,

$$\tau_A = r_p (\mu_0 \rho)^{1/2} / B_0. \tag{12}$$

We divide the velocity into compressible and incompressible parts by writing the velocity field perturbation in terms of scalar and vector potentials via

$$\mathbf{v} = \nabla \times \mathbf{u} + \nabla w, \tag{13}$$

where, by taking the divergence of $\mathbf{v}$, we see that $\mathbf{u}$ is the incompressible component and w is the compressible component of the macroscopic plasma velocity. We also write the magnetic field in terms of a vector potential,

$$\mathbf{b} = \nabla \times \mathbf{a}, \tag{14}$$

so that the criteria $\nabla \cdot \mathbf{b} = 0$ is satisfied for all $\mathbf{a}$. Substituting (13) and (14) into Eqs. (9)–(11) leads to

$$\frac{\partial (\nabla \times \mathbf{u} + \nabla w)}{\partial t} = (\nabla \times \mathbf{B}) \times (\nabla \times \mathbf{a}) + (\nabla \times \nabla \times \mathbf{a}) \times \mathbf{B} - \nabla p, \tag{15}$$

$$\frac{\partial (\nabla \times \mathbf{a})}{\partial t} = \nabla \times ([\nabla \times \mathbf{u} + \nabla w] \times \mathbf{B}) - \nabla \times \eta (\nabla \times \nabla \times \mathbf{a}), \tag{16}$$

$$\frac{\partial p}{\partial t} = -(\nabla \times \mathbf{u} + \nabla w) \cdot \nabla P - \Gamma P \nabla \cdot (\nabla \times \mathbf{u} + \nabla w). \tag{17}$$

Since the stability spectrum can be separated into compressible and incompressible sections, separation of the velocity field equations into their respective parts is desirable. This is achieved by taking the curl and divergence of Eq. (15). It is possible to integrate Eq. (16). Whilst offering a simplification, it also has the effect of introducing a gauge for $\mathbf{a}$ determined by an arbitrary function f, viz.

$$\frac{\partial (\nabla \times \nabla \times \mathbf{u})}{\partial t} = \nabla \times [(\nabla \times \mathbf{B}) \times (\nabla \times \mathbf{a}) + (\nabla \times \nabla \times \mathbf{a}) \times \mathbf{B}], \tag{18}$$

$$\frac{\partial (\nabla^2 w)}{\partial t} = -\nabla^2 p + \nabla \cdot [(\nabla \times \mathbf{B}) \times (\nabla \times \mathbf{a}) + (\nabla \times \nabla \times \mathbf{a}) \times \mathbf{B}], \tag{19}$$

$$\frac{\partial \mathbf{a}}{\partial t} = (\nabla \times \mathbf{u} + \nabla w) \times \mathbf{B} - \eta (\nabla \times \nabla \times \mathbf{a}) + \nabla f, \tag{20}$$

$$\frac{\partial p}{\partial t} = -(\nabla \times \mathbf{u} + \nabla w) \cdot \nabla P - \Gamma P \nabla^2 w, \tag{21}$$

Equations (18)–(21) are the final form of the equations that will be analysed. The choice of the gauge f for $\mathbf{a}$ is an important decision and this can be used to advantage. We have found that choosing f to be equal to $\mathbf{B} \cdot \mathbf{u}$ eliminates any derivatives of $\mathbf{u}$ with respect to the radial flux coordinate (ψ) on the right-hand side of Eq. (20). The direct consequence of this is that there are only algebraic factors of $\mathbf{u}$ when Fourier analysis in the poloidal and toroidal directions is performed, with the resultant numerical advantages. By further testing it was found that introduction of a damping term $h(\psi)$ $(\partial a_\psi / \partial \psi)$ into f provides sufficient attenuation of unwanted numerical oscillations, which otherwise appear. Furthermore, inclusion of this term has the tendency to remove the spurious modes that may have arisen as a consequence of spectral pollution. Although the number of these spurious modes is reduced substantially by the gauge term, they are not entirely eliminated but can be clearly identified by their highly oscilliatory nature which is associated with the number of radial mesh points taken. Some of the remaining spurious modes, which primarily occur near the real ω-axis, disappear when the number of radial mesh points are increased, leaving others whose position on the ω-plane depends on the number of radial grid points, thus giving a pointer to their nature.

By analysing these equations, we can determine both compressible and incompressible spectra in cylindrical and toroidal geometries. The set of equations which correspond to incompressible motion can be obtained by setting $w = 0$ in Eq. (20). Solving Eqs. (18) and (20), with a given equilibrium, for $\mathbf{a}$ and $\mathbf{u}$ would lead to the incompressible solution [2, 3]. Solving Eqs. (18)–(21) simultaneously, with a given equilibrium, for

a, **u**, w, and p provides us with a solution which takes full account of compressibility.

The MHD equilibrium obtained from a solution to the equations of pressure balance ((6)–(8)) defines a natural toroidal coordinate system with nested toroidal flux surfaces defining one of the coordinate surfaces. We use the flux coordinate system in which ψ labels the magnetic surfaces, θ corresponds to the generalised poloidal angle with a period of 2π, whilst ϕ corresponds to the generalised toroidal angle with a period of 2π (Grimm *et al*. [6], Storer [2]). Since the magnetic field lines lie in the flux surfaces ($\mathbf{B} \cdot \nabla\psi = 0$) we can express the equilibrium magnetic field in terms of the flux coordinate system as

$$\mathbf{B} = B_0(f(\psi)\nabla\phi \times \nabla\psi + Rg(\psi)\nabla\phi), \tag{22}$$

where B_0 is identified as the value of the magnetic field at the magnetic axis, R is chosen to be the distance of the magnetic axis from the axis of symmetry, $g(\psi)$ is the toroidal field function, and $f(\psi)$ is the poloidal field function. The choice of Jacobian $\mathcal{J} = c\psi X^2$ defines the poloidal angle θ, where c is a constant adjusted so that the flux coordinate ψ which labels the magnetic surfaces, takes on the values of $\psi = 0$ at the magnetic axis and $\psi = 1$ on the surface. The magnetic field is normalised so that $B_0 = 1$. With this choice of Jacobian the poloidal and toroidal field functions and safety factor $q(\psi)$ are related via

$$f(\psi) = \frac{cRg(\psi)\psi}{q(\psi)}. \tag{23}$$

If we specify the pressure P and toroidal field function g as functions of the poloidal flux, an axisymmetric toroidal equilibrium can be determined numerically by solving the Grad–Shafranov equation,

$$-\Delta^*\Psi = (2\pi)^2 (X^2P' + R^2gg'), \tag{24}$$

which, for the case of toroidal axisymmetry, is a two-dimensional, nonlinear, elliptic, partial differential equation obtained from the reduction of the ideal MHD equilibrium equations ((6)–(8)), where

$$\Delta^* = X\frac{\partial}{\partial X}\frac{1}{X}\frac{\partial}{\partial X} + \frac{\partial^2}{\partial Z^2},$$

with (X, ϕ, Z) being the cylindrical coordinate system used for axisymmetric toroidal equilibria and the prime denoting the partial derivative with respect to the poloidal flux Ψ. We obtain Ψ as a function of X and Z and map this to identify Ψ as a function of the flux coordinate ψ. This enables us to determine P, f, g, and q as functions of the normalised flux coordinate ψ [7].

3. TOROIDAL DECOMPOSITION OF THE EQUATIONS

We can decompose the basic vectors **a** and **u** in terms of their covariant components. Thus we express

$$\mathbf{a} = a_\psi \nabla\psi + a_\theta\nabla\theta + a_\phi \nabla\phi \tag{25}$$

and

$$\mathbf{u} = u_\psi\nabla\psi + u_\theta \nabla\theta + u_\phi \nabla\phi. \tag{26}$$

Each component of the vectors **a** and **u** have a ψ, θ, ϕ, and t dependence. These are Fourier analysed in terms of both the toroidal and poloidal angles. Due to the axisymmetry of the toroidal equilibrium, the toroidal modes decouple and thus can be treated independently. Thus we can specifically write the toroidal components of the perturbed variables as

$$\begin{aligned}
u_\psi(\psi,\theta,\phi,t) &= \sum_l iu_{\psi l}(\psi)\exp(il\theta - in\phi - i\omega t),\\
u_\theta(\psi,\theta,\phi,t) &= \sum_l u_{\theta l}(\psi)\exp(il\theta - in\phi - i\omega t),\\
u_\phi(\psi,\theta,\phi,t) &= \sum_l u_{\phi l}(\psi)\exp(il\theta - in\phi - i\omega t),\\
a_\psi(\psi,\theta,\phi,t) &= \sum_l a_{\psi l}(\psi)\exp(il\theta - in\phi - i\omega t),\\
a_\theta(\psi,\theta,\phi,t) &= \sum_l ia_{\theta l}(\psi)\exp(il\theta - in\phi - i\omega t),\\
a_\phi(\psi,\theta,\phi,t) &= \sum_l ia_{\phi l}(\psi)\exp(il\theta - in\phi - i\omega t),\\
w(\psi,\theta,\phi,t) &= \sum_l iw_l(\psi)\exp(il\theta - in\phi - i\omega t),\\
p(\psi,\theta,\phi,t) &= \sum_l ip_l(\psi)\exp(il\theta - in\phi - i\omega t),
\end{aligned} \tag{27}$$

where l represents the poloidal mode number, n represents the toroidal mode number, t denotes the time dependence of the perturbed variables, and ω denotes the oscillatory frequency of the plasma. The factor i is included explicitly in the analysis so that the real and imaginary terms decouple for up–down symmetry [2]. In this case we need to sum over the various

poloidal components defined by l, to account for the poloidal coupling that is evident in this particular geometry.

Since we are employing non-orthogonal flux coordinates, the vector expressions comprising the basic equations (18)–(21) are neither easy nor trivial to calculate. To perform the vector operations, we need to utilise the standard non-orthogonal vector identities [19, 2]. It is convenient to multiply equations (18)–(21) by the Jacobian $\mathcal{J}$, before performing the Fourier transforms. We have a choice of expanding the vector equations covariantly or contravariantly. For computational simplicity and variable symmetry, we choose to consider the contravariant form of the incompressible velocity vector equation (18) and the covariant form of the magnetic field vector equation (20). Some simplification is possible by using integration by parts to eliminate the θ-derivatives, where possible, and by replacing all ϕ-derivatives of $\mathbf{a}$, $\mathbf{u}$, w, or p by the combination $(-in)$, since their ϕ-dependence is always of the form $e^{-in\phi}$.

After performing the Fourier analysis, the three contravariant components of the curl of the velocity equation,

$$\frac{\partial(\nabla\times\nabla\times\mathbf{u})}{\partial t} = \nabla\times[(\nabla\times\mathbf{B})\times(\nabla\times\mathbf{a}) + (\nabla\times\nabla\times\mathbf{a})\times\mathbf{B}],$$

can be expressed as,

$$\begin{aligned} -i\,\omega\sum_l\sum_\beta\Bigg[&R_{1\alpha\beta}(l',l,\psi)\,u_{\beta l} + R_{2\alpha\beta}(l',l,\psi)\frac{\partial u_{\beta l}}{\partial\psi} \\ &+\frac{\partial}{\partial\psi}(R_{3\alpha\beta}(l',l,\psi)\,u_{\beta l}) + \frac{\partial}{\partial\psi}\left(R_{4\alpha\beta}(l',l,\psi)\frac{\partial u_{\beta l}}{\partial\psi}\right)\Bigg] \\ =\sum_l\sum_\beta\Bigg[&P_{1\alpha\beta}(l',l,\psi)\,a_{\beta l} + P_{2\alpha\beta}(l',l,\psi)\frac{\partial a_{\beta l}}{\partial\psi} \\ &+\frac{\partial}{\partial\psi}(P_{3\alpha\beta}(l',l,\psi)\,a_{\beta l}) + \frac{\partial}{\partial\psi}\left(P_{4\alpha\beta}(l',l,\psi)\frac{\partial a_{\beta l}}{\partial\psi}\right)\Bigg], \end{aligned} \tag{28}$$

while the scalar equation describing the compressible plasma motion (i.e., divergence of the velocity equation),

$$\frac{\partial(\nabla^2 w)}{\partial t} = -\nabla p + \nabla\cdot[(\nabla\times\mathbf{B})\times(\nabla\times\mathbf{a}) + (\nabla\times\nabla\times\mathbf{a})\times\mathbf{B}],$$

takes the form

$$\begin{aligned} -i\,\omega\sum_l\Bigg[&B_1(l',l,\psi)\,w_l + B_2(l',l,\psi)\frac{\partial w_l}{\partial\psi} + \frac{\partial}{\partial\psi}(B_3(l',l,\psi)\,w_l) \\ &+\frac{\partial}{\partial\psi}\left(B_4(l',l,\psi)\frac{\partial w_l}{\partial\psi}\right)\Bigg] \\ =\sum_l\Bigg[&C_1(l',l,\psi)\,p_l + C_2(l',l,\psi)\frac{\partial p_l}{\partial\psi} \\ &+\frac{\partial}{\partial\psi}(C_3(l',l,\psi)\,p_1) + \frac{\partial}{\partial\psi}\left(C_4(l',l,\psi)\frac{\partial p_l}{\partial\psi}\right)\Bigg] \\ &+\sum_l\sum_\beta\Bigg[D_{1\alpha\beta}(l',l,\psi)\,a_{\beta l} + D_{2\alpha\beta}(l',l,\psi)\frac{\partial a_{\beta l}}{\partial\psi} \\ &+\frac{\partial}{\partial\psi}(D_{3\alpha\beta}(l',l,\psi)\,a_{\beta l} + \frac{\partial}{\partial\psi}\left(D_{4\alpha\beta}(l',l,\psi)\frac{\partial a_{\beta l}}{\partial\psi}\right)\Bigg] \\ &+\sum_l\left[\frac{\partial}{\partial\psi}\left(D_5(l',l,\psi)\frac{\partial\xi_l}{\partial\psi}\right) + \frac{\partial}{\partial\psi}\left(D_6(l',l,\psi)\frac{\partial\zeta_l}{\partial\psi}\right)\right], \end{aligned} \tag{29}$$

with the three covariant components of the equation describing the time evolution of the magnetic field via the vector potential $\mathbf{a}$,

$$\frac{\partial\mathbf{a}}{\partial t} = (\nabla\times\mathbf{u}+\nabla w)\times\mathbf{B} - \eta(\nabla\times\nabla\times\mathbf{a}) + \nabla f,$$

being cast as

$$\begin{aligned} -i\,\omega\sum_l\mathcal{J}_{l'-l}(\psi)a_{\alpha l} =&\sum_l\left[A_{1\alpha}(l',l,\psi)\,w_l + A_{2\alpha}(l',l,\psi)\frac{\partial w_l}{\partial\psi}\right] \\ &+\sum_l\sum_\beta[W_{\alpha\beta}(l',l,\psi)\,u_{\beta l}] - \eta\sum_l\sum_\beta\Bigg[Q_{1\alpha\beta}(l',l,\psi)\,\alpha_{\beta l} \\ &+Q_{2\alpha\beta}(l',l,\psi)\frac{\partial a_{\beta l}}{\partial\psi} + \frac{\partial}{\partial\psi}(Q_{3\alpha\beta}(l',l,\psi)\,a_{\beta l}) \\ &+\frac{\partial}{\partial\psi}\left(Q_{4\alpha\beta}(l',l,\psi)\frac{\partial a_{\beta l}}{\partial\psi}\right)\Bigg] \end{aligned} \tag{30}$$

and the scalar equation for the pressure evolution,

$$\frac{\partial p}{\partial t} = -(\nabla\times\mathbf{u}+\nabla w)\cdot\nabla P - \Gamma P\nabla^2 w,$$

is expressed as

$$-i\,\omega \sum_l \mathcal{J}_{l'-l}(\psi) p_l = \sum_l \left[E_1(l', l, \psi)\, w_l + E_2(l', l, \psi) \frac{\partial w_l}{\partial \psi} + \frac{\partial}{\partial \psi}\left(E_3(l', l, \psi)\, w_1\right) + \frac{\partial}{\partial \psi}\left(E_4(l', l, \psi) \frac{\partial w_l}{\partial \psi} \right) \right] + \sum_l \sum_\beta \left[F_{1\beta}(l', l, \psi)\, u_{\beta l} \right], \tag{31}$$

with the auxiliary equations,

$$\sum_l \left(\zeta_l - \frac{\partial a_{\theta l}}{\partial \psi} \right) \delta_{ll'} = 0 \tag{32}$$

and

$$\sum_l \left(\xi_l - \frac{\partial a_{\phi l}}{\partial \psi} \right) \delta_{ll'} = 0, \tag{33}$$

included to avoid third-order radial derivatives, thus preserving the block tridiagonal structure of the problem. The sub-indices α and β take on the values corresponding to the ψ, θ, and ϕ components, ω represents the eigenfrequency, and the sub-indices l and l' label the appropriate Fourier coefficients. It should be noted that one should choose the Fourier component of order $l' - l$ of each coefficient. They take on a range of values $l_{\min} \le l,\ l' \le l_{\max}$ which needs to be increased as we move into toroidal geometry from a circular, cylindrical equilibrium, for which only one value is required. *A*, *B*, *C*, *D*, *E*, *F*, *P*, *Q*, *R*, and *W* are the coefficients of the Fourier components of the perturbed variables. These coefficients are expressed in terms of the Fourier components of various combinations of the metric tensor elements and the Jacobian, along with the functions $f(\psi)$, $g(\psi)$, and $q(\psi)$ and their derivatives. See the Appendix for a listing of these coefficients. In the course of the calculation of the coefficients, it is necessary to carry out numerical differentiation of the metric tensor elements etc. with respect to θ and ψ. The θ derivatives are evaluated employing fast Fourier transform techniques, and the ψ derivatives by using Lagrange interpolation. For a large number of radial mesh points, it is both numerically accurate and computationally efficient to simply interpolate the equilibrium functions and metric tensor elements obtained from the mapping code using a primary radial mesh onto a more finely spaced secondary mesh.

4. BOUNDARY CONDITIONS

As an extension from the large aspect ratio or cylindrical analysis, we can represent the behaviour of the perturbed macroscopic variables at the magnetic axis by

$$\begin{aligned} u_{\psi l},\, a_{\psi l} &\sim \psi^{|\,|l|-1|}, \\ u_{\theta l},\, \mathrm{a}_{\theta l} &\sim \psi^{|\,|l|-1|+1}, \\ u_{\phi l},\, a_{\phi l} &\sim \psi^{|l|}, \\ w_l,\, p_l &\sim \psi^{|l|}, \end{aligned} \tag{34}$$

where l is the poloidal mode number. This result can also be obtained by a full indicial analysis. Casting (34) into more useful form, we have

$$\begin{aligned} \sum_l \left(\frac{\partial a_{\psi l}(\psi)}{\partial \psi} - |\,|l| - 1\,| \frac{a_{\psi l}(\psi)}{\psi} \right) \delta_{ll'} &= 0, \\ \sum_l \left(\frac{\partial a_{\theta l}(\psi)}{\partial \psi} - (|\,|l| - 1\,| + 1) \frac{a_{\theta l}(\psi)}{\psi} \right) \delta_{ll'} &= 0, \\ \sum_l \left(\frac{\partial a_{\phi l}(\psi)}{\partial \psi} - |l| \frac{a_{\phi l}(\psi)}{\psi} \right) \delta_{ll'} &= 0, \\ \sum_l \left(\frac{\partial u_{\psi l}(\psi)}{\partial \psi} - |\,|l| - 1| \frac{u_{\psi l}(\psi)}{\psi} \right) \delta_{ll'} &= 0, \\ \sum_l \left(\frac{\partial u_{\theta l}(\psi)}{\partial \psi} - (|\,|l| - 1| + 1) \frac{u_{\theta l}(\psi)}{\psi} \right) \delta_{ll'} &= 0, \\ \sum_l \left(\frac{\partial u_{\phi l}(\psi)}{\partial \psi} - |l| \frac{u_{\phi l}(\psi)}{\psi} \right) \delta_{ll'} &= 0, \\ \sum_l \left(\frac{\partial w_l(\psi)}{\partial \psi} - |l| \frac{w_l(\psi)}{\psi} \right) \delta_{ll'} &= 0, \\ \sum_l \left(\frac{\partial p_l(\psi)}{\partial \psi} - |l| \frac{p_1(\psi)}{\psi} \right) \delta_{ll'} &= 0 \\ (\psi \Rightarrow 0), & \end{aligned} \tag{35}$$

with the auxiliary equations,

$$\begin{aligned} \sum_l \left(\zeta_l(\psi) - \frac{\partial a_{\theta,l}(\psi)}{\partial \psi} \right) \delta_{ll'} &= 0, \\ \sum_l \left(\xi_l(\psi) - \frac{\partial a_{\phi,l}(\psi)}{\partial \psi} \right) \delta_{ll'} &= 0 \\ (\psi \Rightarrow 0), & \end{aligned}$$

evaluated at the magnetic axis, completing the set of boundary conditions at the origin. l and l' take on all values of l under consideration, where $\delta_{ll'}$ is the Kronecker delta function.

We choose the boundary condition that assumes the plasma

extends to a stationary, perfectly conducting wall. Now the electromagnetic boundary conditions in this case require that the tangential perturbed electric field (i.e., the second and third covariant components of **e**) and normal perturbed magnetic field and velocity vanish on the conducting wall. Using Ohm's law these conditions imply that the second and third covariant components of the perturbed current is zero. We can express these constraints as

$$\begin{aligned}(\nabla \times \mathbf{u})_\psi + (\nabla w)_\psi &= 0,\\ (\nabla \times \mathbf{a})_\psi &= 0,\\ (\nabla \times \nabla \times \mathbf{a})_\theta &= 0,\\ (\nabla \times \nabla \times \mathbf{a})_\phi &= 0\\ (\psi \Rightarrow \psi_p),&\end{aligned} \tag{36}$$

with ψ_p being the value of ψ at the edge of the plasma. Usually ψ_p is taken to be 1. To render the resistive, compressible stability problem in toroidal geometry soluble, we need to solve a system of $10 \times L$ partial differential equations, where $L = l_{\max} - l_{\min} + 1$. Thus to preserve the tridiagonal structure of the numerical problem, we require $10 \times L$ conditions at the boundary of the confined plasma, as we did at the origin. The additional constraints arise from the fact that some of the basic equations contain only first-order spatial derivatives. Thus we need to include these equations at the edge of the plasma column in order to provide us with sufficient conditions. Thus for the perfectly conducting wall we can express the constraints as

$$\sum_l a_{\theta l}(\psi)\delta_{ll'} = 0,$$

$$\sum_l a_{\phi l}(\psi)\delta_{ll'} = 0,$$

$$-i\omega \sum_l \mathcal{J}_{l'-l} a_{\theta l}(\psi) = \sum_l \left[A_{1\theta}(l', l, \psi)\, w_l(\psi) + A_{2\theta}(l', l, \psi) \frac{\partial w_l(\psi)}{\partial \psi} \right] + \sum_l \sum_\beta [W_{\theta\beta}(l', l, \psi)\, u_{\beta l}(\psi)],$$

$$-i\omega \sum_l \sum_\beta \left[R_{1\psi\beta}(l', l, \psi)\, u_{\beta l}(\psi) + R_{2\psi\beta}(l', l, \psi) \frac{\partial u_{\beta l}(\psi)}{\partial \psi} \right] = \sum_l \sum_\beta \left[P_{1\psi\beta}(l', l, \psi)\, a_{\beta l}(\psi) + P_{2\psi\beta}(l', l, \psi) \frac{\partial a_{\beta l}(\psi)}{\partial \psi} \right],$$

$$-i\,\omega \sum_l \mathcal{J}_{l'-l} a_{\psi 1}(\psi) = \sum_l \left[A_{1\psi}(l', l, \psi)\, w_l(\psi) + A_{2\psi}(l', l, \psi) \frac{\partial w_l(\psi)}{\partial \psi} \right] + \sum_l \sum_\beta [W_{\psi\beta}(l', l, \psi)\, u_{\beta l}(\psi)]$$

$$- \eta \sum_l \left[Q_{1\psi\psi}(l', l, \psi)\, a_{\psi l}(\psi) + Q_{2\psi\theta}(l', l, \psi) \frac{\partial a_{\theta l}(\psi)}{\partial \psi} + Q_{2\psi\phi}(l', l, \psi) \frac{\partial a_{\phi l}(\psi)}{\partial \psi} + \frac{\partial}{\partial \psi}(Q_{3\psi\psi}(l', l, \psi)\, a_{\psi l}(\psi)) + \frac{\partial}{\partial \psi}(Q_{4\psi\theta}(l', l, \psi)\, \zeta_l(\psi)) \right],$$

$$\sum_l u_{\phi l}(\psi)\, \delta_{ll'} = 0,$$

$$\sum_l w_l(\psi)\, \delta_{ll'} = 0,$$

$$\sum_l p_l(\psi)\, \delta_{ll'} = 0,$$

$$\sum_l \left(\zeta_l(\psi) - \frac{\partial a_{\theta,l}(\psi)}{\partial \psi} \right) \delta_{ll'} = 0,$$

$$\sum_l \left(\xi_l(\psi) - \frac{\partial a_{\phi,l}(\psi)}{\partial \psi} \right) \delta_{ll'} = 0$$

$$(\psi \Rightarrow \psi_p), \tag{37}$$

for all values of l' under consideration.

With a simple modification, the code can be used to include a vacuum layer surrounding the plasma. In such a region ($\nabla \times \nabla \times \mathbf{a}$) = 0 and we can use the same equations (18)–(21), but with a very large value of η, to simulate this condition.

5. NUMERICAL PROCEDURE

Looking at the central and boundary equations, it is evident that they contain only first- and second-order derivatives of the perturbed macroscopic variables. Taking advantage of this fact, we utilise finite difference techniques and use the radial mesh $\psi_j = \varepsilon + (j - \psi_p)\,\Delta\psi$, with $\Delta\psi = (\psi_p - \varepsilon)/(N - 1)$, j is the mesh index, and ψ_p is the plasma radius. We can define the derivatives using the centred difference formula and recast Eqs. (28)–(31) that describe the interior behaviour of the plasma, into the finite difference form. Thus the interior points ($2 \le j \le N - 1$) can be represented in the matrix form,

$$-i\omega\,(T_{ll',j}\tilde{u}_{l,j-1} + U_{ll',j}\,\tilde{u}_{l,j} + V_{ll',j}\tilde{u}_{l,j+1}) = L_{ll',j}\tilde{u}_{l,j-1} + M_{ll',j}\tilde{u}_{l,j} + N_{ll',j}\tilde{u}_{l,j+1}, \tag{38}$$

where $L_{ll',j}$, $M_{ll',j}$, $N_{ll',j}$, $T_{ll',j}$, $U_{ll',j}$, and $V_{ll',j}$ are square matrices whose order depends on the number of Fourier modes em-

ployed. If $l_{\min} \le l \le l_{\max}$ and $L = l_{\max} - l_{\min} + 1$, then these matrices are of order $10L \times 10L$ which contains the coefficients of the finite differenced variables. $\tilde{u}_{l,j}$ is a column vector containing the perturbed macroscopic variables, viz,

$$\tilde{u}^{\dagger}_{l,j} = (a_{\psi l,j}\, a_{\theta l,j}\, a_{\phi l,j}\, u_{\psi l,j}\, u_{\theta l,j}\, u_{\phi l,j}\, w_{l,j}\, p_{l,j}\, \zeta_{l,j}\, \xi_{l,j}), \tag{39}$$

and ω is the eigenfrequency. The boundary conditions at the origin are represented for $j = 1$ by

$$-i\omega\,(U_{ll',1}\tilde{u}_{l,1} + V_{ll',1}\tilde{u}_{l,2}) = M_{ll',1}\tilde{u}_{l,1} + N_{ll',1}\tilde{u}_{l,2}. \tag{40}$$

Although this equation has been written in a form consistent with (38), the boundary conditions at the origin do not involve ω, so that $U_{ll',1}$ and $V_{ll',1}$ are identically zero. For $j = N$, which treats the boundary conditions imposed at the wall of the contained plasma, we have

$$-i\omega\,(T_{ll',N}\tilde{u}_{,N-1} + U_{ll',N}\tilde{u}_{l,N}) = L_{ll',N}\tilde{u}_{l,N-1} + M_{ll',N}\tilde{u}_{l,N}. \tag{41}$$

One of the advantages in working with the scalar and vector potentials for the velocity (Eq. (13)) is that we are guaranteed that $\nabla \cdot \mathbf{v}$ depends only on the compressible scalar potential w, even when the derivatives are expressed in the finite difference form. This eliminates the problem that occurs when working directly with the components of $\mathbf{v}$ which require different orders of finite differences to represent the derivatives of the radial component, compared with the other components, so that $\nabla \cdot \mathbf{v}$ will be correctly calculated.

Expansion of Eqs. (38), (40), and (41) displays the matrix structure of the problem, which can be expressed via the matrix equation,

$$-i\omega\mathcal{R}\tilde{u} = \mathcal{P}\tilde{u}, \tag{42}$$

where $\mathcal{R}$ and $\mathcal{P}$ are block-tridiagonal matrices of order $10LN \times 10LN$, where $L = l_{\max} - l_{\min} + 1$, and N denotes the number of radial mesh points employed. Thus the spectral analysis is reduced to a general eigenvalue problem, where the eigenvalue ω represents the eigenfrequency of the contained plasma while the eigenvectors $\tilde{u}$ contain the eigenmodes of the macroscopic perturbed variables defined by Eq. (39), i.e.,

$$\tilde{u}\dagger = (\tilde{u}^{\dagger}_{l,1}, \tilde{u}^{\dagger}_{l,2}, ..., \tilde{u}^{\dagger}_{l,N}). \tag{43}$$

The inverse vector iteration procedure, as outlined in Potter [20], provides us with a method of computing both the eigenvalues ω in the complex plane and the corresponding eigenvectors of the eigensystem described by Eq. (42). The method is initialised by choosing a value of ω (say ω_0) which is close to the eigenvalue required, i.e.,

$$\omega = \omega_0 + \Delta\omega, \tag{44}$$

and a guess $\tilde{u}^0$ for the corresponding eigenfunction. Substituting (44) into (42) leads to the iteration procedure

$$(\mathcal{P} + i\omega_0\mathcal{R})\,\tilde{u}^k = -i\,\Delta\omega\mathcal{R}\tilde{u}^{k-1}, \tag{45}$$

with the k^{th} estimate for $\Delta\omega$ given by

$$\Delta\omega = \frac{i\tilde{u}^{k\dagger}\,(\mathcal{P} + i\omega_0\mathcal{R})\,\tilde{u}^k}{\tilde{u}^{k}\dagger\,\mathcal{R}\tilde{u}^k}. \tag{46}$$

This iteration can be continued until the required accuracy is obtained; typically an accuracy of $|\omega^k - \omega^{k-1}| \sim 10^{-10}$ is desired. The amount of c.p.u. time required to converge on a solution is mainly dependent on the initial choice of ω_0. The iterative equation can be expressed as

$$\mathcal{D}\tilde{u} = W, \tag{47}$$

where $\mathcal{D}$ is a block-tridiagonal matrix, W is a column vector, and $\tilde{u}$ is the solution column vector.

Equations of this type can be solved without requiring the whole matrix to be held in memory at one time (Potter [20]; Storer [2]) and we avoid the obstacle of being required to calculate the inverses of large matrices, which is very time consuming. Using this algorithm gives us an expedient method for solving the block-tridiagonal matrix equation (47) and, hence, a technique to perform the iterative procedure defined by Eq. (45). Thus we have a succinct method for locating the eigenfrequencies ω in the complex plane and their corresponding eigenfunctions. The amount of c.p.u. time required to locate each eigenvalue depends on the accuracy of the initial guess ω_0. On the Fujitsu VP220 at the Australian National University one iteration with 200 radial points and 7 poloidal modes takes about 2 s c.p.u. time and 10 iterations are commonly required. Thus it is highly desirable for our approximation of the eigenvalue to have at least some degree of accuracy. To account for the toroidicity of typical toroidal systems in our analysis, we are required to employ a finite number of poloidal harmonics. This leads to very large matrices. For example, if we choose to use 10 harmonics and 100 radial mesh points ($L = 10$, $N = 100$), the matrices $\mathcal{R}$ and $\mathcal{P}$ have dimensions 10000×10000. The alternative package eigenvalue solvers (based on the QR algorithm) we could employ an effective limit of around 1000×1000. To solve directly eigenvalue problems involving matrices with larger dimensions than this is unrealistic. In order to obtain a first approximation to the full eigenvalue spectrum, we have to compromise between the number of mesh points and the number of harmonics used; i.e., we need to satisfy, $N \times L \sim 100$. We often run the package solver (i.e., the QR algorithm) which finds all the eigenvalues for individual poloidal harmonic values and then employ the inverse iteration

code to link together the harmonics. While this method does not give us a good approximation to the toroidal spectrum, it at least provides us with a good starting point for the point spectrum values in the complex frequency plane and gives a very good indication that we have not missed significant eigenvalues.

VALIDATION

A fundamental aspect of every computational research program is a testing of the numerical code at various limits to ensure validation. SPECTOR is essentially a toroidal spectral code that is capable of being employed with compressible, incompressible, resistive, or ideal assumptions, in geometries ranging from toroids to cylinders, with arbitrarily shaped poloidal cross sections. In order to have confidence in SPECTOR's results, we need to validate the code with these assumptions and limits in mind.

A magnetohydrodynamic equilibrium is determined by a number of factors, including the shape of the poloidal cross section, the aspect ratio, the pressure, and the safety factor profiles. The associated eigenspectrum will therefore depend on these factors in a complex way. The first test will be for a constant current model at a large aspect ratio with circular cross section, which has an analytic solution [21]. For this model the eigenspectrum depends only on the dimensionless quantities nq_0 and κ, defined by

$$\kappa = \frac{nr_p}{R_m}. \tag{48}$$

The Solov'ev equilibrium [22] is equivalent to this model in the large aspect ratio limit. To test the validity of our toroidal spectral code we execute SPECTOR, employing a Solov'ev equilibrium at large aspect ratio, and compare the resultant spectrum with the spectra obtained from the purely cylindrical analysis. In comparing various equilibria related to this model, it is useful to choose parameters so that the values of nq_0 and κ remain the same. The parameters used for the large aspect ratio test are as follows: $l = 1$, $n = 50$, $R = 150$, $g_0 = 1$, $q_0 = 0.032$. This corresponds to $\kappa = \frac{1}{3}$ and $nq_0 = 1.6$. To test SPECTOR in the *incompressible*, resistive case, we set $w_l = 0$ in Eqs. (28)–(31). Figure 1 displays in the complex ω-plane the stable frequency spectrum obtained for $\eta = 5 \times 10^{-5}$. This compares well with the analytic spectrum obtained from Storer [21] for this model. The stable part of the spectrum forms two pairs of lines that originate near the real ω-axis on either side of the ideal accumulation point $|\omega_A| = 0.125$, initially run parallel to and below the real ω-axis, and then arc below until they converge and meet the lower part of the imaginary ω-axis at approximately $-i\omega_A$. Figure 2 shows an enhanced view of the lines near the real ω-axis. For this case no instabilities exist on the positive imaginary ω-axis; however an indefinite number of super-stable modes were found accumulating on the negative

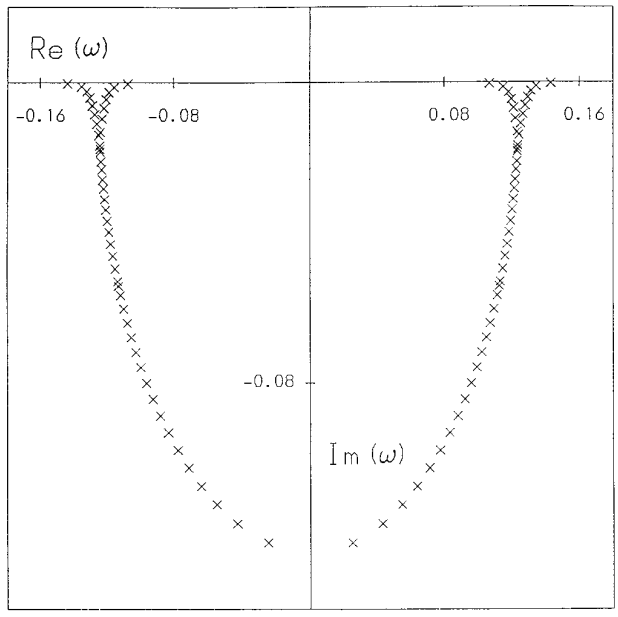

FIG. 1. Eigenfrequency spectrum for incompressible constant current model with modified boundary conditions.

imaginary ω-axis. For clarity we have chosen not to display them.

The direct consequence of a change in resistivity is an increase in the density of the spectral points on the characteristic eigenvalue lines. To quantify this change in density of eigenvalues we referred to the analytical treatment of an exactly soluble resistive cylindrical MHD model [21]. The frequency spectrum can be found from

$$i\omega\,(i\omega - \eta\,(\zeta^2 + \kappa^2)) = \left(\frac{B_p}{B_0}\right)^2 \left[-(l - nq)^2 \pm \frac{2|l - nq|\kappa}{\sqrt{\zeta^2 + \kappa^2}}\right], \tag{49}$$

with ζ taking on a series of values corresponding to zeros of the transcendental equation,

$$\kappa\zeta J_m'(\zeta) \pm (\zeta^2 + \kappa^2)^{1/2}\, mJ_m(\zeta) = 0. \tag{50}$$

The quadratic equation (49) will have a real part only if

$$4\left(\frac{B_p}{B_0}\right)^2 \left[-(l - nq)^2 \pm \frac{2|l - nq|\kappa}{\sqrt{\zeta^2 + \kappa^2}}\right] > \eta^2\,(\zeta^2 + \kappa^2)^2.$$

If this condition is satisfied there will be two solutions in the third and fourth quadrants of the Argand diagram, as we have seen in Fig. 1. Now consider two successive values of ω which correspond to values of ζ which differ by about π (since the transcendental equation involves Bessel functions) and

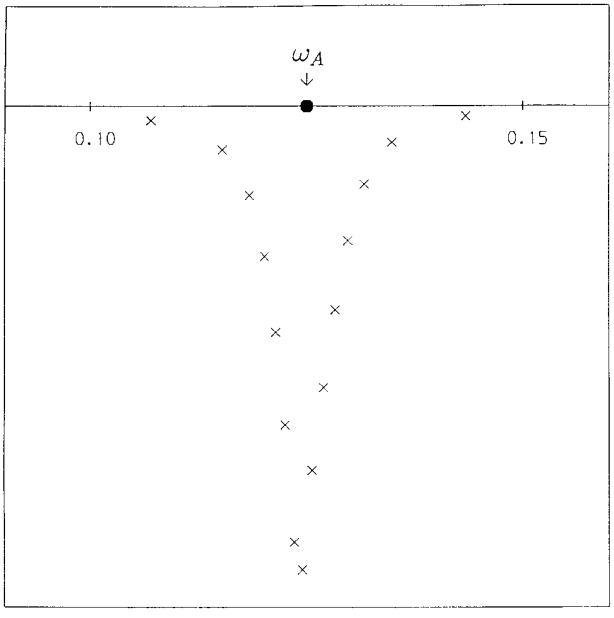

FIG. 2. Enhanced view of characteristic lines near ω_A.

which have approximately the same *real* values. The distance between them can then be written as

$$|\omega_{i+1} - \omega_i| \simeq \left| \frac{\eta}{2}(\zeta_0^2 + \kappa^2) - \frac{\eta}{2}((\zeta_0 + \pi)^2 + \kappa^2) \right| \simeq \frac{\eta}{2}(\zeta_0 2\pi + \pi^2).$$

Now $\Im(\omega_i) = (\eta/2)(\zeta_0^2 + \kappa^2)$; therefore we can write $\zeta_0 = \sqrt{2\Im(\omega_i)/\eta - \kappa^2}$. Thus for small resistivity η we can express the distance between successive eigenvalues as

$$|\omega_{i+1} - \omega_i| \simeq \sqrt{\eta}\,\sqrt{2\pi^2 \Im(\omega_i)}. \tag{51}$$

Equation (51) implies that the density or spacing of the eigenvalues on the characteristic lines depends on the resistivity and specifically varies as $\sqrt{\eta}$. We see that this result is consistent with the theory of Dewar and Davies [13] and Pao and Kerner [11]. To verify this numerically we considered the equilibrium as described above, varied the resistivity from $1 \times 10^{-5} < \eta < 1 \times 10^{-3}$, and calculated the distance between successive eigenvalues on a particular characteristic line for each value of η. Figure 3 depicts eigenvalue density versus $\sqrt{\eta}$ which indicates the $\sqrt{\eta}$ dependence with the correct coefficient.

To test SPECTOR in the *compressible*, non-constant current, cylindrical limit we need to include the compressible part of the velocity in the analysis ($w \neq 0$) and deal with an equilibrium which possesses a non-constant current in the toroidal direction. We simulate this by choosing the toroidal field function and safety factor to ensure that they possess quadratic profiles. Figure 4 displays the following equilibrium quantities: current J_ϕ, magnetic field B_θ, toroidal field function $g(\psi)$, safety function $q(\psi)$, poloidal field function $f(\psi)$, and pressure $P(\psi)$. We use $l = 1$, $n = 50$, $R = 150$ (so that $nq_0 = 1.6$), and $\eta = 5 \times 10^{-5}$ with the number of radial mesh points $N \sim 501$. For the *compressible* case the stable spectra have three branches—Alfvén, slow magneto-acoustic, and fast magneto-acoustic. Figure 5 shows the Alfvén and slow magneto-acoustic eigenfrequency spectra in the complex ω-plane. A direct consequence of the equilibrium possessing a non-constant current in the toroidal direction is a bifurcation in the Alfvén characteristic eigenvalue lines near the real ω-axis. The endpoints of the lines are given in terms of,

$$\omega_A(\psi) = \frac{r_p}{Rq(\psi)}\,|l - nq(\psi)|. \tag{52}$$

If the safety factor $q(\psi)$ is constant, the ideal Alfvén continuum collapses to a point and bifurcation in the resistive Alfvén spectrum does not occur. However, if $q(\psi)$ varies with ψ then the range of the ideal Alfvén continuum determines the endpoints of the bifurcation in the resistive spectrum. These bifurcation lines make an angle of approximately 60° and 45° with the real ω-axis which is consistent with the theory of Dewar and Davies [13]. The stable spectrum, as before, is located in the third and fourth quadrants of the Argand diagram. Starting at the ideal continuum endpoints ($\omega_A(0)$, $\omega_A(\psi_p)$), the Alfvén characteristic lines then arc down towards the negative imaginary axis.

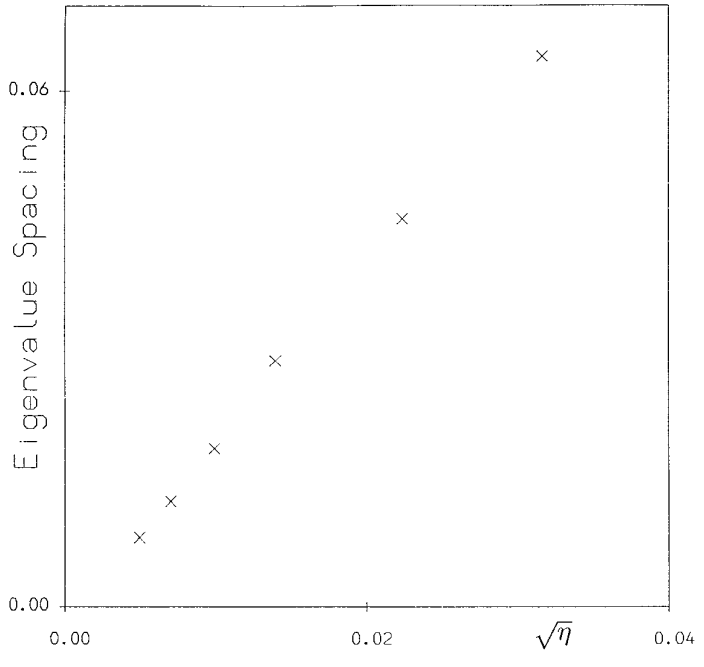

FIG. 3. Graph of eigenvalue density vs. $\sqrt{\eta}$.

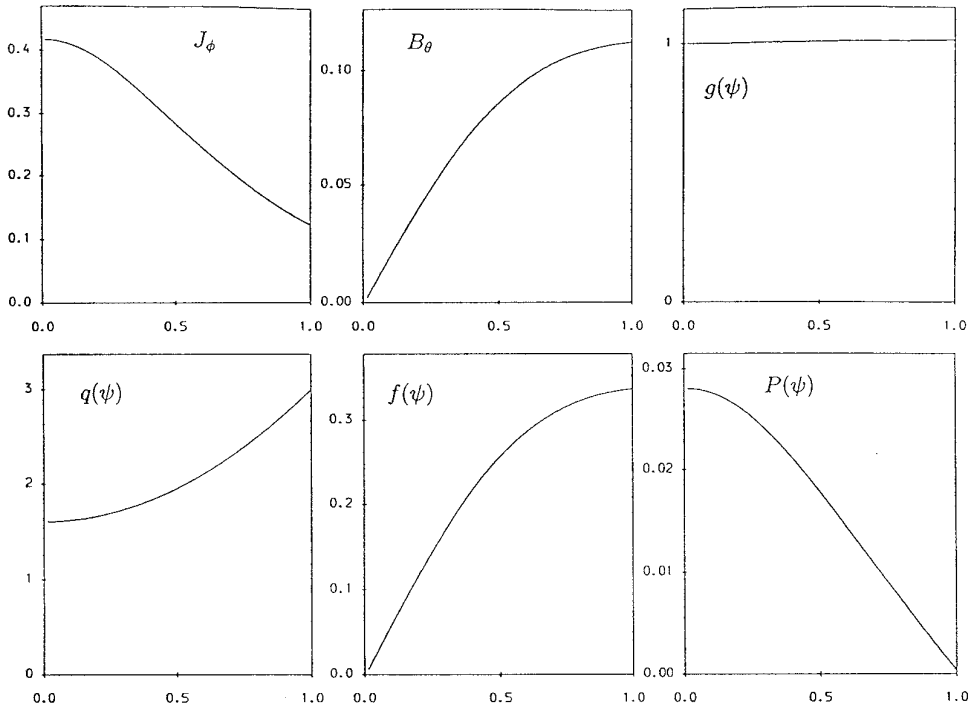

FIG. 4. Equilibrium quantities for non-constant current model.

As is evident from Fig. 5, the slow magneto-acoustic spectrum is located at lower frequency than the Alfvén spectrum. The endpoints are defined in terms of the Alfvén frequency ω_A by

$$\omega_{SM}(0) = \left(\frac{\Gamma}{\Gamma + q^2(0)R^2}\right)^{1/2} \omega_A(0) \qquad (53)$$

$$\omega_{SM}(r_p) = 0.$$

The effect of introducing a non-constant current on the slow sound spectrum is a change in the angles that the bifurcated lines make with the real ω-axis. See Fig. 6. Angles of about 10° and 80° are subtended by these lines. The characteristic lines associated with the slow magneto-acoustic spectrum then arc down towards the negative imaginary axis. An indefinite number of super-stable modes are also evident on the negative imaginary ω-axis. The fast magneto-acoustic waves have a frequency too high to appear in these diagrams. Figures 7 and 8 show the poloidal projections of the perturbed velocity **v** for the associated eigenfrequencies ''a'' and ''b.'' It is interesting to note that the eigenfunctions on the left-hand side of the bifurcation are concentrated near the magnetic axis and on the right-hand side of the bifurcation they are concentrated near the edge of the plasma column, as observed by Ryu and Grimm [9].

To further test the code SPECTOR, we turn our attention to a toroidal low aspect ratio case and test the ideal parts of the code against data from the ERATO code [6] and other codes. The incompressible ERATO results were published in Hughes *et al*. [3] and Storer [2] and were obtained by executing ERATO with a large value of the ratio of specific heats Γ. The compressible ERATO results were quoted in Chance *et al*. [5]. We work with a Solov'ev equilibrium, in which the equilibrium current is strictly inversely proportional to the distance from the central

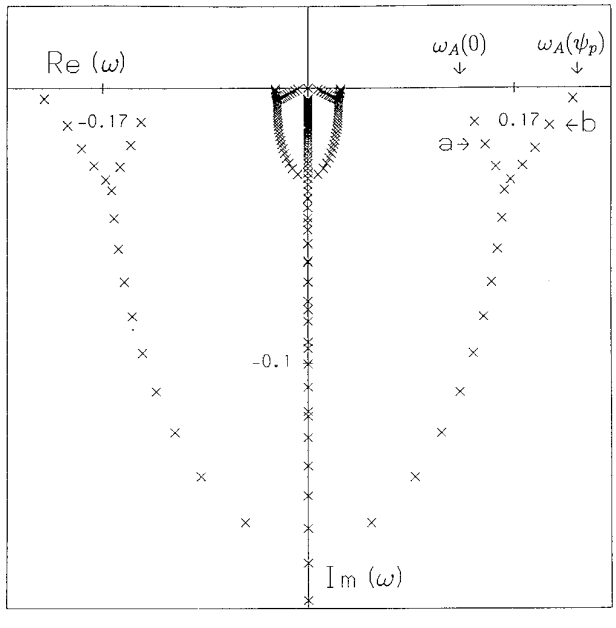

FIG. 5. Eigenfrequency spectrum for compressible non-constant current model.

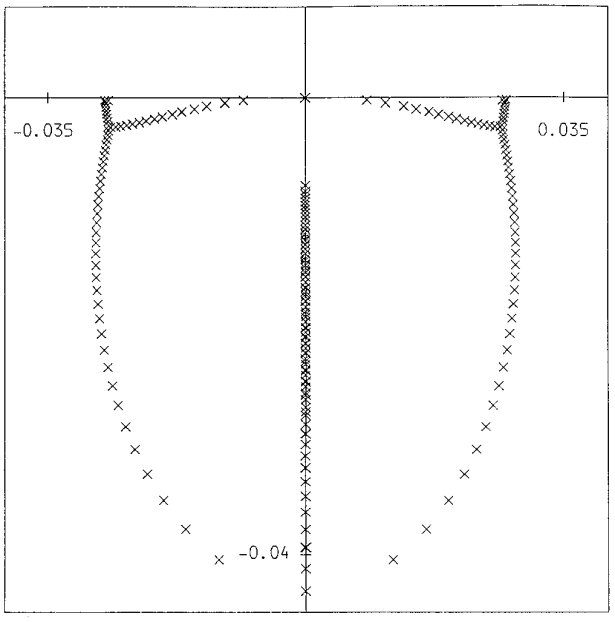

FIG. 6. Details of slow magneto-sonic spectrum.

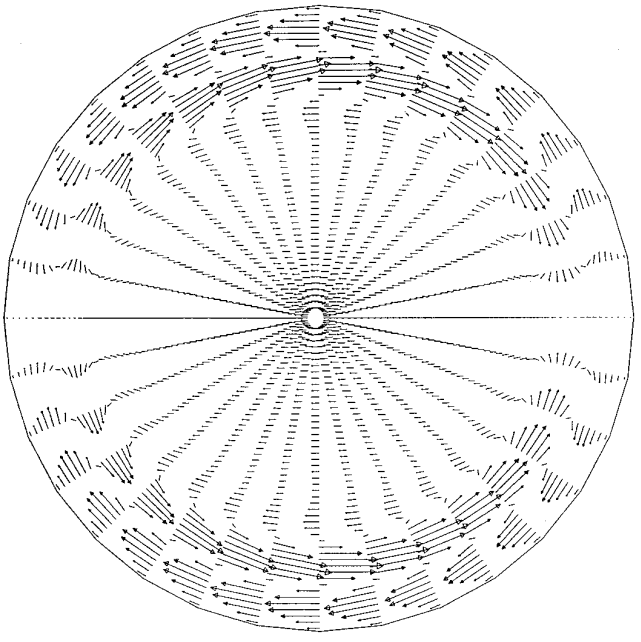

FIG. 8. Poloidal velocity projection for eigenvalue ''b.''

axis [22]. This type of equilibrium is a simple model which corresponds to the constant current model in the cylindrical limit and embodies most of the essential features of ''real'' toroidal equilibria, including finite aspect ratio and elongated poloidal cross-sectional shape. Employment of Solov'ev equilibria allows for direct comparison between toroidal and cylindrical results, providing we maintain the values of κ and nq. Furthermore, this equilibrium has an analytic form for the poloidal flux, making it easier to map into the relevant coordinate system. Two cases are considered: $E = 2$, which provides an elongated D-shaped plasma, and $E = 1$, which yields an almost circular plasma with a slight D-shaped deformation, with varying ranges of poloidal and toroidal mode numbers l and n, for ideal, incompressible and compressible plasmas. The model employed assumes that the plasma column extends to a stationary, perfectly conducting wall.

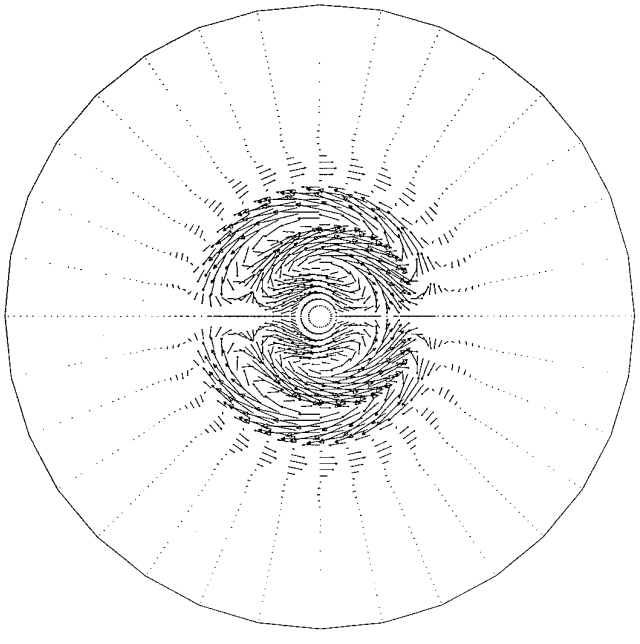

FIG. 7. Poloidal velocity projection for eigenvalue ''a.''

For the first case, we consider Solov'ev equilibria which have an aspect ratio $R/a = 3$, toroidal mode number $n = 2$, and ellipticity $E = 2$, with values of the safety factor at the magnetic axis varying from $0.1 \leq q_0 \leq 1.1$. Figure 9 displays the flux surfaces for this particular equilibrium. Note the elongated D-shape of the equilibrium. Employing SPECTOR in the ideal, incompressible limit, by setting $w_l = 0$ and $\eta = 0$ in Eqs. (28)–(31), we execute the code with the number of radial mesh points $N = 101$ and utilise 11 poloidal harmonics with $-4 \leq l \leq 6$, $-3 \leq l \leq 7$, and $-2 \leq l \leq 8$, depending on the safety factor's range. It proved useful to centre the poloidal modes around the dominant mode number, which can be estimated before the calculation, since usually $nq(0) < l_{\text{dominant}} < nq(\psi_p)$, for a case where q is a monotonically increasing function. For each equilibria corresponding to a different value of $q(0)$, we search for the fastest growing mode (i.e., instability) along the positive imaginary axis of the ω plane. Figure 10 depicts the most unstable mode growth rates as a function of $q(0)$, where $\Omega^2 = -\omega^2 q^2(\psi_p)\mathrm{R}^2$, with Ω^2 denoting the square of the growth rate in units of the poloidal Alfvén frequency (using the poloidal field at the surface of the plasma), where ω is the complex eigenfrequency (obtained from SPECTOR) in units of the toroidal Alfvén frequency (using the toroidal

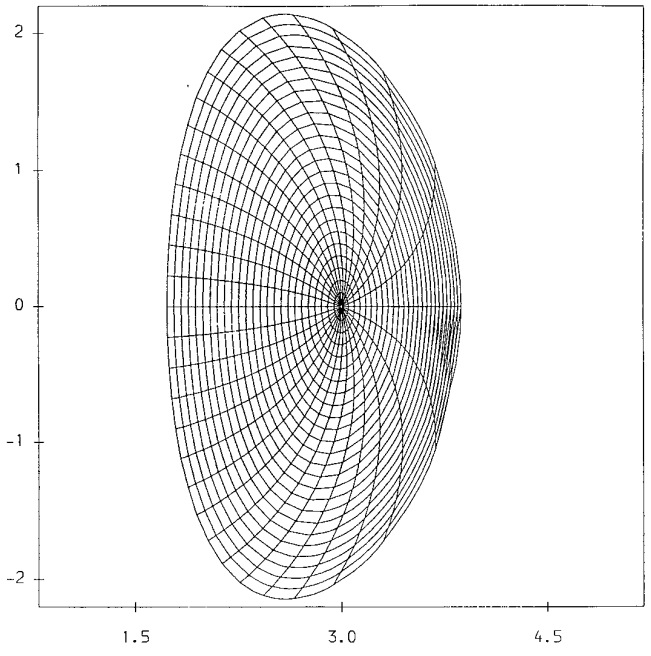

FIG. 9. Surfaces of constant flux for equilibrium with $R/a = 3$, $E = 2$, $n = 2$.

field at the magnetic axis), $q(\psi_p)$ is the value of the safety factor at the boundary of the plasma, and R is the major radius. Note that many singular surfaces, corresponding to $l - nq = 0$, exist due to the shear of the safety factor. From Fig. 10 it is evident that three resonances or peaks exist although the last two are rather weak.

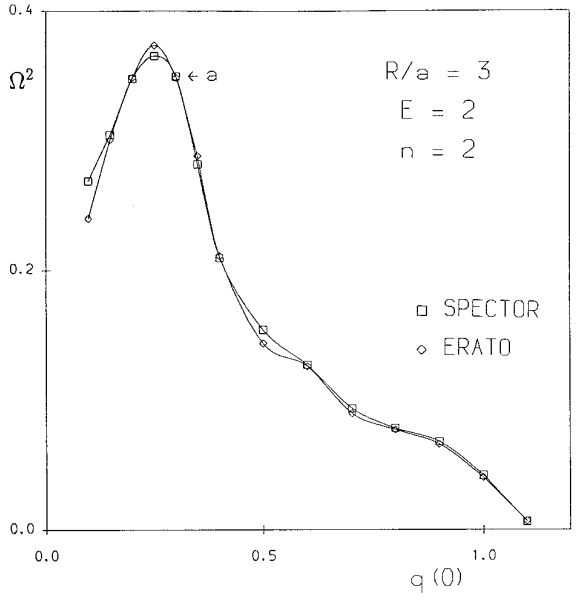

FIG. 10. Comparison between SPECTOR and ERATO of the ideal, $n = 2$ mode growth rates as a function of $q(0)$ for the Solov'ev equilibrium.

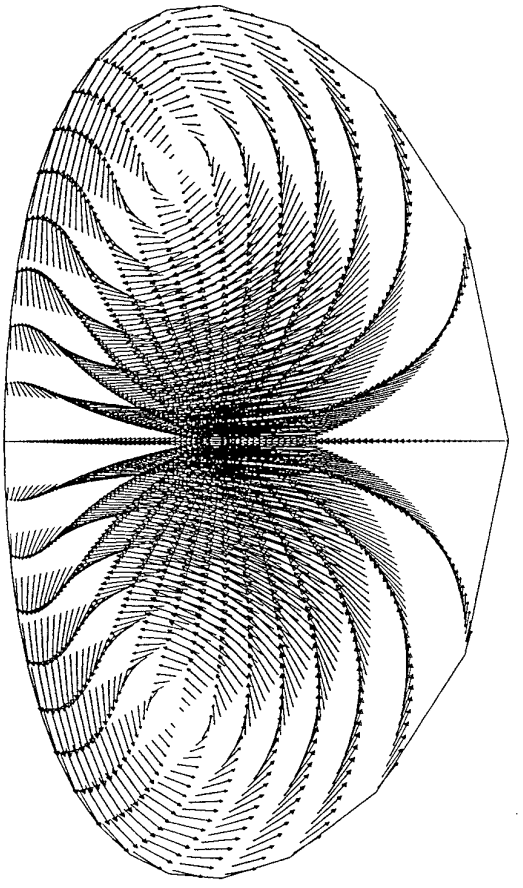

FIG. 11. Poloidal velocity projection for eigenvalue ''a.''

To compare this toroidal, *incompressible*, ideal limit, output from ERATO [6] was superimposed against our results, Fig. 10. As is evident there is good agreement between the two codes. It is important to note that since we utilised eleven poloidal harmonics in the analysis, for computational efficiency we only employed $N = 101$ radial mesh points. Increasing N refines the agreement between SPECTOR and ERATO. Reconstruction of the eigenfunctions proves useful for the interpretation of results and assists in the understanding of the physical nature of the eigenmodes. SPECTOR has this facility built into the code. Reconstructing the perturbed physical variables from the Fourier coefficients contained in the eigenvector $\tilde{u}^{\dagger}_{l,j}$, as defined by Eq. (39), by utilising the harmonic expansions (27) and Eqs. (13) and (14), we can view the poloidal projections of these quantities. For example, Fig. (11) displays the poloidal projection of the perturbed velocity $\mathbf{v}$ corresponding to the unstable eigenfrequency ''a,'' which is in the neighbourhood of the main resonance, as labelled on Fig. 10. Figure 12 shows the relative poloidal harmonic contributions to $\mathbf{v}$, averaged (in a root mean square sense) over all flux surfaces, for the instability. There is generally a dominant poloidal mode for each eigenmode, with decreasing contributions from neighbouring harmonics. From perusal of Figs. 11 and 12 it is evident that instability ''a,'' which is near the main peak or resonance, is

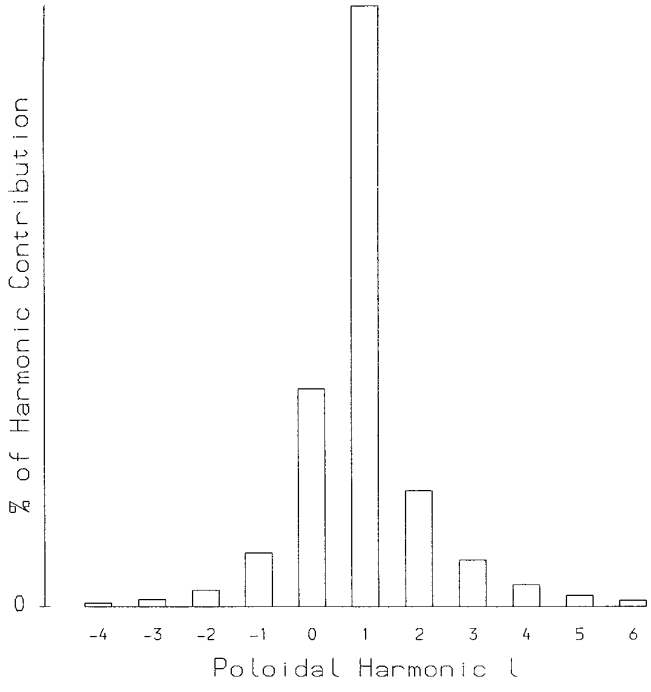

FIG. 12. Poloidal harmonic contribution to **v** for eigenvalue ''a.''

dominated by the $l = 1$ harmonic with significant contributions from the $l = -1$, $l = 0$, and $l = 2$ harmonics, which is reflected in the poloidal projections.

To display the validity of SPECTOR for the toroidal ideal *compressible* case, we consider the above equilibrium ($R/a = 3$, $E = 2$, $n = 2$) and execute SPECTOR with $w_l \neq 0$ and $\eta = 0$ in Eqs. (28)–(31), using $N = 151$ radial mesh points and eleven poloidal harmonics with $-4 \leq l \leq 6$. We ran the code for two particular values of $q(0)$ and compared with compressible data from KERNER, PEST, and ERATO, obtained from Chance *et al.* [23]. Table I displays the comparison between the codes.

From Table I we can see that the results from SPECTOR are in good agreement with the other existing toroidal codes. Thus we can conclude that SPECTOR accurately calculates the ideal unstable spectrum for both compressible and incompressible toroidal plasmas.

It is of interest to note the effect of including various numbers

TABLE I

Comparison of Specific Compressible Results for Ω^2

$\frac{R}{a}$	E	$q(0)$	$q(\psi_p)$	n	KERNER	PEST	ERATO	SPECTOR
3	2	0.3	0.523	2	0.413	0.427	0.431	0.4319
3	2	0.7	1.22	2	0.118	0.119	0.120	0.1178

Note. The square of the growth rate $\Omega^2 = -\omega^2 q^2(\psi_p)R^2$, where ω is obtained directly from SPECTOR, for the Solov'ev model with $N = 151$.

TABLE II

Eigenvalue for Low Aspect Ratio Solov'ev Case

l_{max} \ l_{min}	0	−1	−2	−3	−4
1	0.076153	0.075649	0.075336	0.075508	0.075621
2	0.123124	0.123824	0.123734	0.123793	0.123837
3	0.131331	0.132252	0.132169	0.132215	0.132252
4	0.134178	0.135253	0.135182	0.135227	0.135263
5	0.135188	0.136345	0.136281	0.136325	0.136361
6	0.135532	0.136723	0.136661	0.136706	0.136742
7	0.135641	0.136844	0.136785	0.136835	

Note. The magnitude of the eigenvalue, as a function of the poloidal harmonics used, for a low aspect ratio Solov'ev case ($R/a = 3$, $n = 2$, $E = 1$, $N = 101$, $q(0) = 0.4$). For comparison the ERATO result is $-i\omega = 0.1367$.

of poloidal modes and radial mesh points. Table II illustrates the effect of increasing the number of poloidal modes L ($= l_{max} - l_{min} + 1$) with various values of l_{min} and l_{max} for the case where $q(0) = 0.4$ for the second equilibrium with $E = 1$. Note the eigenvalue as obtained by ERATO is $-i\omega = 0.1367$. From Table II we can see that convergence is not uniform with increasing l_{max}; however, it is evident that the result for nine poloidal harmonics centred on $l = 1$ is unlikely to change by more than 0.4% by including more poloidal modes.

One would expect that as we increase N the discrepancy between the numerical and analytic result would decrease. The finite difference procedures employed to simulate the continuum and approximate the spatial derivatives of the perturbed variables are second-order accurate so that the numerical result should differ from the analytic result by an amount of order $(\Delta\psi)^2$, where $\Delta\psi = (\psi_p - \varepsilon)/(N - 1)$. These results are illustrated in Fig. 13, where we used the above model with $N = 41$, 51, 61, 71, 81, 91, 101, and 151, and $-4 \leq l \leq 6$ for $q(0) = 0.4$. It is evident that the effect of increasing N is indeed a refinement in the agreement between the numerical and analytic result. Figure 13 suggests that a realistic comparison with the analytic result should only be made after extrapolation.

TOROIDALLY INDUCED RESISTIVE ALFVÉN EIGENMODES

A consequence of increasing the toroidicity of the plasma under consideration is a gradual increase in the poloidal harmonic coupling prevalent in the associated eigenmodes. However, this is not the only observed effect. Recent studies of the stable shear Alfvén spectrum for toroidal plasmas, using the ideal MHD model, have led to the discovery of the discrete toroidicity-induced Alfvén eigenmodes (TAE modes) by Cheng and Chance [24]. These were further investigated by Poedts and Schwarz [25], Turnbull *et al.* [26], Ye *et al.* [27], and others. The toroidal coupling effects due to a nonuniform magnetic field over a magnetic surface can cause interactions among the

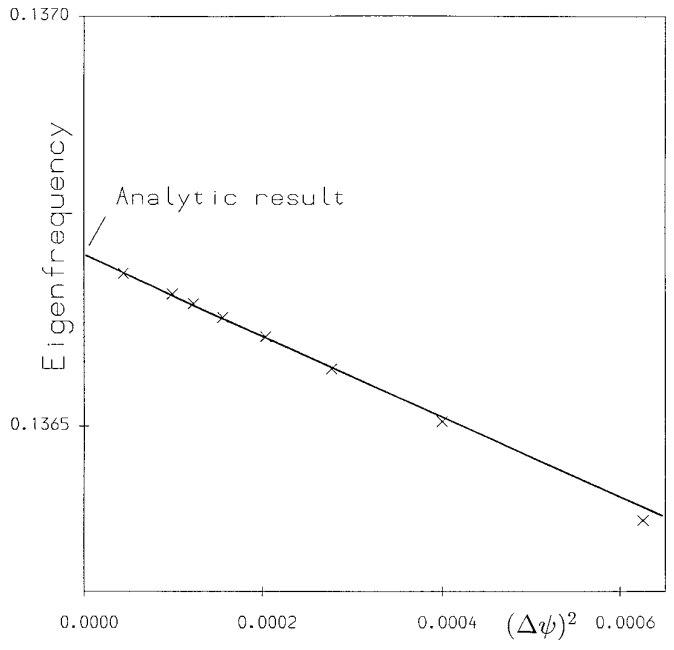

FIG. 13. Comparison between the analytic result and the numerical result extrapolated to $\Delta\psi = 0$. The linear part of the curve corresponds to values of $N \geq 50$.

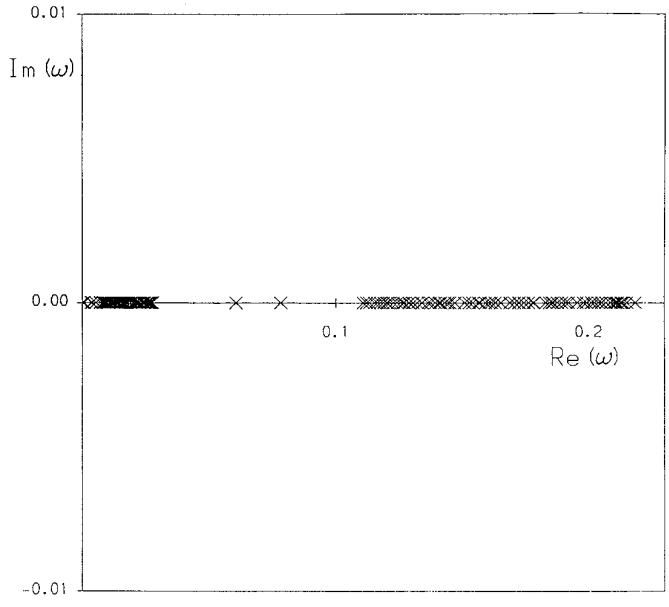

FIG. 14. Ideal eigenfrequency spectrum for an equilibrium with aspect ratio 4. Note the toroidally induced gap and the toroidal Alfvén eigenmodes marked with an *x*.

neighbouring poloidal harmonics and can break up the ideal shear Alfvén continuous spectrum resulting in continuum gaps. The size of these gaps depends on the strength of the poloidal mode coupling and the appearance of the gaps stresses the importance of the two-dimensional effects. When the poloidal mode coupling is strong enough, ideal global Alfvén eigenmodes can be found with frequencies inside the continuum gaps. The existence of these toroidicity-induced shear Alfvén eigenmodes suggests a new efficient Alfvén wave-heating scheme. These modes might play an important role in controlled thermonuclear fusion as they may be destabilised by interaction with fusion born α-particles (Cheng *et al.* [28, 29], Wong *et al.* [30]).

To demonstrate this phenomenon, using SPECTOR to show the effect of resistive damping on these global Alfvén modes, we considered an equilibrium with aspect ratio $R/a = 4$, ellipticity $E = 1$, toroidal mode number $n = 1$, with an approximately quadratic safety factor such that $1.04 \leq q(\psi) \leq 2.833$. Employing SPECTOR first as an ideal MHD code, by setting $\eta = 0$ in Eqs. (28)–(31), we ran the code with the number of radial mesh points $N = 101$ and $N = 151$ and utilised eight poloidal harmonics with $-1 \leq l \leq 6$. The shear in the $q(\psi)$ profile causes the magnetic field to possess a non-uniform structure over the radial domain, which in turn enhances poloidal harmonic coupling. Figure 14 displays the Alfvén eigenfrequency spectrum in the complex ω-plane then obtained. The $l = 1$ and $l = 2$ ideal continua are evident along the real ω-axis. In the large aspect ratio analysis, these continua would overlap. Due to the toroidicity of the current equilibrium strong poloidal harmonic coupling exists. A direct consequence of this interaction of neighbouring poloidal modes is the formation of the continuum gap, as well as the emergence of two isolated global TAE modes, marked with crosses in the gap, as is consistent with current theory (Poedts and Schwarz [0], Turnbull et al. [26]).

To test the effect of introducing finite resistivity on these global modes, we steadily increased η from $\eta = 0$ to a highly resistive case $\eta = 10^{-2}$ in a study of the TAE mode in Fig. 14 with the smallest value of Re(ω). As was intuitively expected, the direct consequence of increasing the resistivity of the model was the introduction of damping in these modes, indicated by a ''pulling down'' of the eigenmodes from the real ω-axis. Figure 15, plotting the negative imaginary part of the eigenfrequency against the $-\log(\eta)$ depicts this departure from the real ω-axis, which is consistent with the work by Poedts *et al.* [25]. Features of this graph are the two plateau regions between $10^{-5} \leq \eta \leq 10^{-3}$ and $10^{-9} \leq \eta \leq 3 \times 10^{-7}$. It should be noted that this resistive damping is very weak and may not overcome other destabilising mechanisms. We do not have an explanation for this interesting behaviour which, at least at the smallest values of η, may take the numerical procedure beyond the limits of its validity for the largest number of radial grid points that we were able to use.

8. CONCLUSION

Interest in the results of resistive MHD analysis of toroidal plasmas remains high, as many of the gross macroscopic properties of these plasmas are described well by this model. It is

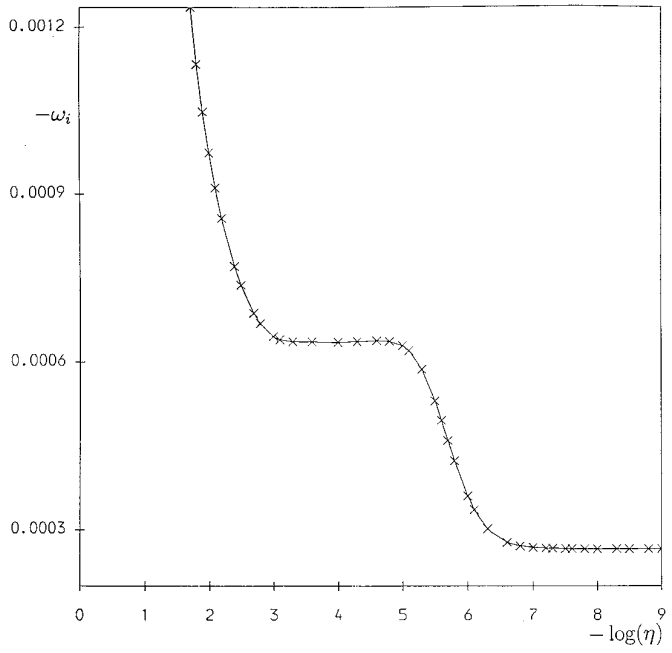

FIG. 15. The resistively induced damping of the TAE mode as a function of η.

therefore useful to have access to a range of numerical codes which can provide us with information, not only of the unstable modes and the range of parameters which lead to stability, but also of the stable part of the spectrum. Interaction between the plasma and externally imposed electromagnetic fields can be illuminated by a detailed study of the stable spectrum and this information may be of importance in studies of diagnostic procedures and heating mechanisms. As mentioned in the last section, toroidicity and shaping may lead to new classes of modes (TAE and EAE modes) which may be of real significance in the analysis of fusion devices. We hope that the code we have developed may be able to contribute to these developments.

APPENDIX: COEFFICIENTS OF MHD EQUATIONS FOR TOROIDAL GEOMETRY

$$A_{1\psi} = -lg_{\psi\psi}Rg - \frac{nf\mathcal{T}}{X^2}, \quad A_{2\psi} = -ig_{\psi\theta}Rg,$$

$$A_{1\theta} = ilg_{\theta\psi}Rg, \quad A_{2\theta} = -g_{\theta\theta}Rg,$$

$$A_{1\phi} = \frac{-ilfg_{\phi\phi}g_{\psi\theta}}{\mathcal{T}}, \quad A_{2\phi} = \frac{g_{\phi\phi}g_{\theta\theta}f}{\mathcal{T}}$$

$$B_1 = -ll'g_{\phi\phi}\frac{g_{\psi\psi}}{\mathcal{T}} - \mathcal{T}\frac{n^2}{X^2}, \quad B_2 = -il'g_{\phi\phi}\frac{g_{\theta\psi}}{\mathcal{T}},$$

$$B_3 = -ilg_{\phi\phi}\frac{g_{\psi\theta}}{\mathcal{T}}, \quad B_4 = \frac{g_{\phi\phi}g_{\theta\theta}}{\mathcal{T}}$$

$$C_1 = -ll'g_{\phi\phi}\frac{g_{\psi\psi}}{\mathcal{T}} + \mathcal{T}\frac{n^2}{X^2}, \quad C_2 = il'g_{\phi\phi}\frac{g_{\theta\psi}}{\mathcal{T}},$$

$$C_3 = ilg_{\phi\phi}\frac{g_{\psi\theta}}{\mathcal{T}}, \quad C_4 = \frac{g_{\phi\phi}g_{\theta\theta}}{\mathcal{T}}$$

$$D_{1\psi} = -inl'Y_{\psi\theta} - ill'Y_{\theta\psi} - \frac{n^2}{X^2}\left(l'Rg + nf\frac{g_{\theta\theta}}{\mathcal{T}}\right) + \frac{ilnf}{X^2}\frac{\partial}{\partial\theta}\left(\frac{g_{\phi\phi}}{\mathcal{T}}\right) - \frac{nl^2f}{\mathcal{T}}$$

$$D_{1\theta} = -nl'Y_{\psi\psi} + \frac{n^2}{X^2}\frac{\partial(Rg)}{\partial\psi} + \frac{in^3fg_{\theta\psi}}{\mathcal{T}X^2},$$

$$D_{1\phi} = -ll'Y_{\psi\psi} + \frac{nl}{X^2}\frac{\partial(Rg)}{\partial\psi} + \frac{iln^2fg_{\theta\psi}}{\mathcal{T}X^2},$$

$$D_{2\psi} = -l'g_{\phi\phi}\frac{g_{\theta\psi}}{\mathcal{T}^2}\left(\frac{nfg_{\theta\theta}}{\mathcal{T}} + lRg\right),$$

$$D_{2\theta} = il'Y_{\phi\psi} - nl'fg_{\phi\phi}g_{\theta\psi}\frac{g_{\theta\psi}}{\mathcal{T}^3} - i\frac{\partial}{\partial\psi}\left(\frac{l'g_{\phi\phi}g_{\theta\psi}Rg}{\mathcal{T}^2}\right) - \frac{inf}{X^2}\frac{\partial}{\partial\theta}\left(\frac{g_{\phi\phi}}{\mathcal{T}}\right) + \frac{nlf}{\mathcal{T}},$$

$$D_{2\phi} = -il'Y_{\psi\theta} - \frac{n}{X^2}\left(l'Rg + \frac{nfg_{\theta\theta}}{\mathcal{T}}\right) - ll'g_{\phi\phi}g_{\theta\psi}\frac{fg_{\theta\psi}}{\mathcal{T}^3} + i\frac{\partial}{\partial\psi}\left(l'fg_{\phi\phi}g_{\theta\psi}\frac{g_{\theta\theta}}{\mathcal{T}^3}\right),$$

$$D_{3\psi} = nY_{\theta\theta} + lY_{\phi\theta}, \quad D_{3\theta} = -inY_{\theta\psi} + \frac{n^2Rg}{X^2},$$

$$D_{3\phi} = -ilY_{\theta\psi} + \frac{nlRg}{X^2},$$

$$D_{4\psi} = \frac{g_{\phi\phi}g_{\theta\theta}}{\mathcal{T}^2}\left(\frac{nfg_{\theta\theta}}{\mathcal{T}} + lRg\right),$$

$$D_{4\theta} = -Y_{\phi\theta} - ig_{\phi\phi}\frac{g_{\theta\psi}}{\mathcal{T}^2}\left(\frac{nfg_{\theta\theta}}{\mathcal{T}} - l'Rg\right),$$

$$D_{4\phi} = Y_{\theta\theta} - i(l+l')fg_{\phi\phi}g_{\theta\theta}\frac{g_{\theta\psi}}{\mathcal{T}^3}, \quad D_5 = -g_{\phi\phi}g_{\theta\theta}\frac{Rg}{\mathcal{T}^2},$$

$$D_6 = g_{\phi\phi}g_{\theta\theta}\frac{fg_{\theta\theta}}{\mathcal{T}^3}$$

$$E_1 = \Gamma P\left(ll'g_{\phi\phi}\frac{g_{\psi\psi}}{\mathcal{T}} + \frac{n^2\mathcal{T}}{X^2}\right) - ilg_{\phi\phi}\frac{g_{\psi\theta}}{\mathcal{T}}\left(\frac{\partial(\Gamma P)}{\partial\psi} - \frac{\partial P}{\partial\psi}\right),$$

$$E_2 = i\Gamma Pl'g_{\phi\phi}\frac{g_{\theta\psi}}{\mathcal{T}} + \frac{g_{\phi\phi}g_{\theta\theta}}{\mathcal{T}}\left(\frac{\partial(\Gamma P)}{\partial\psi} - \frac{\partial P}{\partial\psi}\right),$$

$$E_3 = i\Gamma P l g_{\phi\phi}\frac{g_{\psi\theta}}{\mathcal{T}}, \quad E_4 = -\Gamma P g_{\phi\phi}\frac{g_{\theta\theta}}{\mathcal{T}},$$

$$F_{1\theta} = -n\frac{\partial P}{\partial \psi}, \quad F_{1\phi} = -l\frac{\partial P}{\partial \psi}$$

$$P_{1\psi\psi} = \left(n^2\frac{fg_{\theta\theta}}{\mathcal{T}^2} - ilZ_{\phi\phi}\right)(l' - nq), \quad P_{1\psi\theta} = -nl'Z_{\phi\psi} + n^2 Z_{\theta\psi},$$
$$P_{1\psi\phi} = -ll'Z_{\phi\psi} + nlZ_{\theta\psi}, \quad P_{2\psi\theta} = iZ_{\phi\phi}(l' - nq),$$
$$P_{2\psi\phi} = \frac{nfg_{\theta\theta}}{\mathcal{T}^2}(l' - nq),$$

$$P_{1\theta\psi} = -n^2 Z_{\psi\theta} + lnZ_{\psi\phi}, \quad P_{1\theta\theta} = in^2 Z_{\psi\psi}, \quad P_{1\theta\phi} = inlZ_{\psi\psi},$$
$$P_{2\theta\theta} = -nZ_{\psi\phi},$$
$$P_{2\theta\phi} = -nZ_{\psi\theta}, \quad P_{3\theta\psi} = lZ_{\phi\theta}, \quad P_{3\theta\theta} = nZ_{\phi\psi}, \quad P_{3\theta\phi} = lZ_{\phi\psi},$$
$$P_{4\theta\theta} = -Z_{\phi\theta}$$
$$P_{1\phi\psi} = -nl'Z_{\psi\theta} + ll'Z_{\psi\theta}, \quad P_{1\phi\theta} = inl'Z_{\psi\psi}, \quad P_{1\phi\phi} = ill'Z_{\psi\psi},$$
$$P_{2\phi\theta} = -l'Z_{\psi\phi},$$

$$P_{2\phi\phi} = -l'Z_{\psi\theta,}\ P_{3\phi\psi} = \frac{nfg_{\theta\theta}}{\mathcal{T}^2}(l' - nq) - ilZ_{\theta\phi} + ll'\frac{Rg}{\mathcal{T}},$$

$$P_{3\phi\theta} = nZ_{\theta\psi},$$

$$P_{3\phi\phi} = lZ_{\theta\psi}, \quad P_{4\phi\theta} = \frac{-l'Rg}{\mathcal{T}} + iZ_{\theta\phi}, \quad P_{4\phi\phi} = \frac{fg_{\theta\theta}}{\mathcal{T}^2}(l' - nq)$$

$$Q_{1\psi\psi} = ll'g_{\psi\psi}\frac{g_{\phi\phi}}{\mathcal{T}} + \frac{ilg_{\phi\phi}}{\mathcal{T}}\frac{\partial g_{\psi\psi}}{\partial\theta} + \frac{n^2\mathcal{T}}{X^2} - il\frac{g_{\phi\phi}}{\mathcal{T}}\frac{\partial g_{\psi\theta}}{\partial\psi},$$

$$Q_{2\psi\theta} = -l'g_{\psi\psi}\frac{g_{\phi\phi}}{\mathcal{T}} - \frac{ig_{\phi\phi}}{\mathcal{T}}\frac{\partial g_{\psi\psi}}{\partial\theta} + \frac{ig_{\phi\phi}}{\mathcal{T}}\frac{\partial g_{\psi\theta}}{\partial\psi},$$

$$Q_{2\psi\theta} = \frac{n\mathcal{T}}{X^2}, \quad Q_{3\psi\psi} = \frac{ilg_{\psi\theta}g_{\phi\phi}}{\mathcal{T}},$$

$$Q_{4\psi\theta} = \frac{-ig_{\phi\phi}g_{\psi\theta}}{\mathcal{T}}, \quad Q_{1\theta\psi} = -ill'\frac{g_{\theta\psi}g_{\phi\phi}}{\mathcal{T}} + \frac{lg_{\phi\phi}}{\mathcal{T}}\frac{\partial g_{\theta\psi}}{\partial\theta} - \frac{lg_{\phi\phi}}{\mathcal{T}}\frac{\partial g_{\theta\theta}}{\partial\psi},$$

$$Q_{1\theta\theta} = \frac{n^2\mathcal{T}}{X^2}, \quad Q_{1\theta\phi} = \frac{nl\mathcal{T}}{X^2}, \quad Q_{2\theta\theta} = il'g_{\theta\psi}\frac{g_{\phi\phi}}{\mathcal{T}} - \frac{g_{\phi\phi}}{\mathcal{T}}\frac{\partial g_{\theta\psi}}{\partial\theta} + \frac{g_{\phi\phi}}{\mathcal{T}}\frac{\partial g_{\theta\theta}}{\partial\psi},$$

$$Q_{3\theta\psi} = \frac{lg_{\theta\theta}g_{\phi\phi}}{\mathcal{T}}, \quad Q_{4\theta\theta} = \frac{-g_{\theta\theta}g_{\phi\phi}}{\mathcal{T}},$$

$$Q_{1\phi\psi} = inl'g_{\phi\phi}\frac{g_{\psi\theta}}{\mathcal{T}} - \frac{ng_{\psi\theta}}{\mathcal{T}}\frac{\partial g_{\phi\phi}}{\partial\theta} + \frac{ng_{\theta\theta}}{\mathcal{T}}\frac{\partial g_{\phi\phi}}{\partial\psi},$$

$$Q_{1\phi\theta} = nl'g_{\phi\phi}\frac{g_{\psi\psi}}{\mathcal{T}} + \frac{ing_{\psi\psi}}{\mathcal{T}}\frac{\partial g_{\phi\phi}}{\partial\theta} - \frac{ing_{\theta\psi}}{\mathcal{T}}\frac{\partial g_{\phi\phi}}{\partial\psi},$$

$$Q_{1\phi\phi} = ll'g_{\phi\phi}\frac{g_{\psi\psi}}{\mathcal{T}} + \frac{ilg_{\psi\psi}}{\mathcal{T}}\frac{\partial g_{\phi\phi}}{\partial\theta} - \frac{ilg_{\theta\psi}}{\mathcal{T}}\frac{\partial g_{\phi\phi}}{\partial\psi},$$

$$Q_{2\phi\phi} = il'g_{\phi\phi}\frac{g_{\psi\theta}}{\mathcal{T}} - \frac{g_{\psi\theta}}{\mathcal{T}}\frac{\partial g_{\phi\phi}}{\partial\theta} + \frac{g_{\theta\theta}}{\mathcal{T}}\frac{\partial g_{\phi\phi}}{\partial\psi},$$

$$Q_{3\phi\psi} = -ng_{\phi\phi}\frac{g_{\theta\theta}}{\mathcal{T}}, \quad Q_{3\phi\theta} = ing_{\phi\phi}\frac{g_{\theta\psi}}{\mathcal{T}},$$

$$Q_{3\phi\phi} = ilg_{\phi\phi}\frac{g_{\theta\psi}}{\mathcal{T}}, \quad Q_{4\phi\phi} = \frac{-g_{\phi\phi}g_{\theta\theta}}{\mathcal{T}}$$

$$R_{1\psi\psi} = \frac{n^2 g_{\theta\theta}}{\mathcal{T}} + \frac{ll'g_{\phi\phi}}{\mathcal{T}}, \quad R_{1\psi\theta} = \frac{in^2 g_{\theta\psi}}{\mathcal{T}},$$
$$R_{1\psi\phi} = \frac{inlg_{\theta\psi}}{\mathcal{T}}, \quad R_{2\psi\theta} = \frac{l'g_{\phi\phi}}{\mathcal{T}},$$
$$R_{2\psi\phi} = \frac{-ng_{\theta\theta}}{\mathcal{T}}, \quad R_{1\theta\psi} = \frac{-in^2 g_{\psi\theta}}{\mathcal{T}},$$
$$R_{1\theta\theta} = \frac{n^2 g_{\psi\psi}}{\mathcal{T}}, \quad R_{1\theta\phi} = \frac{nlg_{\psi\psi}}{\mathcal{T}},$$
$$R_{2\theta\phi} = \frac{ing_{\psi\theta}}{\mathcal{T}}, \quad R_{3\theta\psi} = \frac{-lg_{\phi\phi}}{\mathcal{T}}, \quad R_{4\theta\theta} = \frac{-g_{\phi\phi}}{\mathcal{T}},$$
$$R_{1\phi\psi} = \frac{-il'ng_{\psi\theta}}{\mathcal{T}}, \quad R_{1\phi\theta} = \frac{nl'g_{\psi\psi}}{\mathcal{T}},$$
$$R_{1\phi\phi} = \frac{ll'g_{\psi\psi}}{\mathcal{T}}, \quad R_{2\phi\phi} = \frac{il'g_{\psi\theta}}{\mathcal{T}},$$
$$R_{3\phi\psi} = \frac{ng_{\theta\theta}}{\mathcal{T}}, \quad R_{3\phi\theta} = \frac{ing_{\theta\psi}}{\mathcal{T}}, \quad R_{3\theta\theta} = \frac{ilg_{\theta\psi}}{\mathcal{T}}, \quad R_{4\phi\phi} = \frac{-g_{\theta\theta}}{\mathcal{T}}$$

$$W\psi\psi = -f(l - ng), \quad W_{\psi\theta} = \mathcal{T}\frac{\partial}{\partial\psi}\left(\frac{f}{\mathcal{T}}\right),$$
$$W_{\psi\phi} = \mathcal{T}\frac{\partial}{\partial\psi}\left(\frac{qf}{\mathcal{T}}\right),$$
$$W_{\theta\theta} = f(l - nq) + \frac{if}{\mathcal{T}}\frac{\partial\mathcal{T}}{\partial\theta}, \quad W_{\theta\phi} = \frac{iqf}{\mathcal{T}}\frac{\partial\mathcal{T}}{\partial\theta},$$
$$W_{\phi\phi} = f(l - nq), \tag{54}$$

where the factors Y_{ij} and Z_{ij} are given by,

$$Y_{\psi\psi} = \frac{g_{\phi\phi}}{\mathcal{T}^2}\left[g_{\psi\psi}\left\{\frac{\partial}{\partial\psi}\left(\frac{g_{\theta\theta}f}{\mathcal{T}}\right) - \frac{\partial}{\partial\theta}\left(\frac{g_{\psi\theta}f}{\mathcal{T}}\right)\right\} + fg_{\psi\theta}\left\{\frac{\partial}{\partial\psi}\left(\frac{g_{\theta\psi}}{\mathcal{T}}\right) - \frac{\partial}{\partial\theta}\left(\frac{g_{\psi\psi}}{\mathcal{T}}\right)\right\} - \frac{ilfg_{\theta\psi}g_{\psi\psi}}{\mathcal{T}}\right]$$

$$Y_{\psi\theta} = \frac{g_{\phi\phi}}{\mathcal{T}^2}\left[g_{\psi\theta}\left\{\frac{\partial}{\partial\psi}\left(\frac{g_{\theta\theta}f}{\mathcal{T}}\right) - \frac{\partial}{\partial\theta}\left(\frac{g_{\psi\theta}f}{\mathcal{T}}\right)\right\} + fg_{\psi\theta}\left\{\frac{\partial}{\partial\psi}\left(\frac{g_{\theta\theta}}{\mathcal{T}}\right)\right.\right.$$

$$- \frac{\partial}{\partial\theta}\left(\frac{g_{\theta\psi}}{\mathcal{J}}\right)\Bigg\} - \frac{ilfg_{\psi\theta}g_{\theta\psi}}{\mathcal{J}}\Bigg]$$

$$Y_{\theta\psi} = \frac{g_{\phi\phi}}{\mathcal{J}^2}\Bigg[g_{\theta\psi}\left\{\frac{\partial}{\partial\psi}\left(\frac{g_{\theta\theta}f}{\mathcal{J}}\right) - \frac{\partial}{\partial\theta}\left(\frac{g_{\psi\theta}f}{\mathcal{J}}\right)\right\} + fg_{\theta\theta}\left\{\frac{\partial}{\partial\psi}\left(\frac{g_{\theta\psi}}{\mathcal{J}}\right) - \frac{\partial}{\partial\theta}\left(\frac{g_{\psi\psi}}{\mathcal{J}}\right)\right\} - \frac{ilfg_{\psi\psi}g_{\theta\theta}}{\mathcal{J}}\Bigg]$$

$$Y_{\theta\theta} = \frac{g_{\phi\phi}}{\mathcal{J}^2}\Bigg[g_{\theta\theta}\left\{\frac{\partial}{\partial\psi}\left(\frac{g_{\theta\theta}f}{\mathcal{J}}\right) - \frac{\partial}{\partial\theta}\left(\frac{g_{\psi\theta}f}{\mathcal{J}}\right)\right\} + fg_{\theta\theta}\left\{\frac{\partial}{\partial\psi}\left(\frac{g_{\theta\theta}}{\mathcal{J}}\right) - \frac{\partial}{\partial\theta}\left(\frac{g_{\psi\theta}}{\mathcal{J}}\right)\right\} - \frac{ilfg_{\psi\theta}g_{\theta\theta}}{\mathcal{J}}\Bigg]$$

$$Y_{\phi\psi} = \frac{1}{\mathcal{J}}\left[g_{\theta\psi}\frac{\partial}{\partial\psi}\left(\frac{Rgg_{\phi\phi}}{\mathcal{J}}\right) - Rgg_{\psi\psi}\frac{\partial}{\partial\theta}\left(\frac{g_{\phi\phi}}{\mathcal{J}}\right) - \frac{ilRgg_{\phi\phi}g_{\psi\psi}}{\mathcal{J}}\right]$$

$$Y_{\phi\theta} = \frac{1}{\mathcal{J}}\left[g_{\theta\theta}\frac{\partial}{\partial\psi}\left(\frac{Rgg_{\phi\phi}}{\mathcal{J}}\right) - Rgg_{\psi\theta}\frac{\partial}{\partial\theta}\left(\frac{g_{\phi\phi}}{\mathcal{J}}\right) - \frac{ilRgg_{\phi\phi}g_{\psi\theta}}{\mathcal{J}}\right]$$

$$Z_{\psi\psi} = \frac{ifg_{\psi\psi}(l-nq)}{\mathcal{J}^2} + \frac{f}{\mathcal{J}}\frac{\partial}{\partial\theta}\left(\frac{g_{\psi\psi}}{\mathcal{J}}\right) + \frac{g_{\theta\psi}}{\mathcal{J}}\frac{\partial}{\partial\psi}\left(\frac{f}{\mathcal{J}}\right),$$

$$Z_{\psi\theta} = \frac{ifg_{\psi\theta}(l-nq)}{\mathcal{J}^2} + \frac{2}{\mathcal{J}}\frac{\partial}{\partial\theta}\left(\frac{g_{\psi\theta}f}{\mathcal{J}}\right) + \frac{g_{\theta\theta}}{\mathcal{J}}\frac{\partial}{\partial\psi}\left(\frac{f}{\mathcal{J}}\right) - \frac{1}{\mathcal{J}}\frac{\partial}{\partial\psi}\left(\frac{g_{\theta\theta}f}{\mathcal{J}}\right),$$

$$Z_{\psi\phi} = \frac{Rg}{\mathcal{J}X^2}\frac{\partial g_{\phi\phi}}{\partial\psi} = \frac{1}{\mathcal{J}}\frac{\partial(Rg)}{\partial\psi} - \frac{g_{\phi\phi}}{\mathcal{J}}\frac{\partial}{\partial\psi}\left(\frac{Rg}{X^2}\right),$$

$$Z_{\theta\psi} = \frac{-ifg_{\theta\psi}}{\mathcal{J}^2}(l'-nq) - \frac{1}{\mathcal{J}}\left[\frac{\partial}{\partial\psi}\left(\frac{g_{\theta\theta}f}{\mathcal{J}}\right) - \frac{\partial}{\partial\theta}\left(\frac{g_{\psi\theta}f}{\mathcal{J}}\right)\right],$$

$$Z_{\theta\phi} = \frac{-Rg}{X^2}\frac{\partial}{\partial\theta}\left(\frac{g_{\phi\phi}}{\mathcal{J}}\right) - \frac{ilRg}{\mathcal{J}}, Z_{\phi\psi} = \frac{1}{\mathcal{J}}\frac{\partial(Rg)}{\partial\psi},$$

$$Z_{\phi\theta} = \frac{if}{\mathcal{J}}\frac{\partial}{\partial\theta}\left(\frac{g_{\phi\phi}}{\mathcal{J}^2}\right) - \frac{fg_{\phi\phi}}{\mathcal{J}^2}(l-nq), Z_{\phi\phi} = \frac{f}{\mathcal{J}}\frac{\partial}{\partial\theta}\left(\frac{g_{\phi\phi}}{\mathcal{J}}\right) + \frac{ilfg_{\phi\phi}}{\mathcal{J}^2}, \tag{54}$$

where l and n are the poloidal and toroidal mode numbers, $f(\psi)$ and $g(\psi)$ are the poloidal and toroidal field functions, $q(\psi)$ is the safety factor, $g_{ij}(\psi,\theta)$ are the contravariant metric tensor elements, R is the major radius of the toroid, P is the equilibrium pressure, Γ is the ratio of specific heats, and $\mathcal{J}(\psi,\theta)$ is the Jacobian of transformation. Note that any cyclic terms not included in the above lists are identically zero.

ACKNOWLEDGMENTS

The authors are grateful to the other members of the plasma physics group at Flinders University. Financial support was provided by an Australian Post-graduate Research Award and through the Australian Research Grants Scheme and the Australian National University Supercomputer Facility.

REFERENCES

1. L. A. Charlton, J. A. Holmes, H. R. Hicks, V. E. Lynch, and B. A. Carreras, *J. Comput. Phys.* **63,** 107 (1986).
2. R. G. Storer, *J. Comput. Phys.* **66,** 294 (1986).
3. M. H. Hughes, M. W. Philips, and R. G. Storer, *Comput. Phys. Commun.* **72,** 76 (1992).
4. G. Vlad, H. Lütjens, and A. Bondeson, (1991) ''Controlled Fusion and Plasma Heating,'' in *Proceedings, 18th European Conference, Berlin* (EPS, Geneva, 1991), Vol. 15C, Part iv, p. 85.
5. W. Kerner, S. Poedts, J. P. Goedbloed, G. T. A. Huysmans, B. Keegan, and E. Schwarz, (1991). *Proceedings 18th European Conference on Controlled Fusion and Plasma Physics, Berlin*(EPS, Geneva, 1991), Part iv, p.89.
6. R. Gruber, F. Troyon, D. Berger, L. C. Bernard, S. Rousset, R. Schreiber, W. Kerner, W. Schneider, and K. V. Roberts *Comput. Phys. Commun.* **21,** 323 (1981).
7. R. C. Grimm, J. M. Greene, and J. L. Johnson, *Methods Comput. Phys.* **16,** 253 (1976).
8. H. R. Strauss, *Phys. Fluids* **20,** 1354 (1977).
9. C. M. Ryu, and R. C. Grimm, *J. Plasma Phys.* **32,** 207 (1984).
10. W. Kerner, and K. Lerbinger, *Phys. Fluids* **29,** 9 (1986).
11. Y. P. Pao, and W. Kerner, *Phys. Fluids* **28,** 287 (1984).
12. W. Kerner, K. Lerbinger, R. Gruber, and T. Tsunematsu, (1985) *Comput. Phys. Commun.* **36,** 225 (1985).
13. R. L. Dewar, and B. Davies, *J. Plasma Phys.* **32,** 443 (1984).
14. C. Z. Cheng, and M. S. Chance, *J. Comput. Phys.* **71,** 124 (1987).
15. S. Poedts, W. Kerner, J. P. Goedbloed, B. Keegan, G. T. A. Huysmans, and E. Schwarz, *Plasma Phys. Controlled Fusion* **34,** 8, 1397 (1992).
16. A. D. Turnbull, E. J. Strait, W. W. Heidbrink, M. S. Chu, H.H. Duong, J. M. Greene, L. L. Lao, T. S. Taylor, and S. J. Thompson, *Phys. Fluids B* **5,** 2546 (1993).
17. W. Kerner, D. Borba, G. T. A. Huysmans, F. Porcelli, S. Poedts, J. P. Goedbloed, and R. Betti, *Plasma Phys. Controlled Fusion* **36,** 911 (1994).
18. A. R. Schellhase, Ph.D dissertation, Flinders University of South Australia, 1994 (unpublished).
19. G. Bateman, *M. H. D. Instabilities* (MIT Press, Cambridge, MA, 1978).
20. D. Potter, *Computational Physics* (Wiley-Interscience, New York, 1973).
21. R. G. Storer, *Plasma Phys.* **25,**1279 (1983).
22. L. S. Solov'ev, *Sov. Phys.-JETP* **26,** 400 (1968).
23. M. S. Chance, J. M. Greene, R. C. Grimm, J. L. Johnson, J. Manikham, W. Kerner, D. Berger, L. C. Bernard, R. Gruber, and F. Troyon, *J. Comput. Phys.* **28,** 1 (1978).
24. C. Z. Cheng, and M. S. Chance, *Phys. Fluids* **29,** 11 (1986).
25. S. Poedts, and E. Schwarz, *J. Comput. Phys.* **105,** 165 (1993).
26. A. D. Turnbull, M. S. Chu, M. S. Chance, J. M. Greene, L. L. Lao, and E. J. Strait, *Phys. Fluids B* **4,** 3451 (1992).
27. H. Ye, Z. Sedlacek, and S. M. Mahajan, *Phys. Fluids B* **5,** 8, 2999 (1993).
28. C. Z. Cheng, L. Chen, and M. S. Chance, *Ann. of Phys.* **161,** 21 (1985).
29. C. Z. Cheng, R. B. White, G. Y. Fu, L. Chen, D. J. Sigmar, C. T. Hsu, A. Beklemishev, H. L. Berk, B. Breizman, S. C. Guo, Z. Guo, D. Lindberg, and J. W. Van Dam, *Plasma Physics Laboratory,* No. PPPL-2730, Princeton Univ., 1991 (unpublished).
30. K. L. Wong, *et al. Plasma Physics Laboratory,* No. PPPL-2740, Princeton Univ., 1991 (unpublished).